

**Quasiparticle electronic structure and optical response  
( $G_0W_0$ +BSE) of anatase  $\text{TiO}_2$  starting from modified HSE06  
functionals**

Sruthil Lal S.B and Alok Sharan\*

*Department of Physics, Pondicherry University,  
R. V. Nagar, Kalapet, Puducherry, India*

D Murali

*Indian Institute of Information Technology Design and Manufacturing (IIITDM),  
Kurnool, Andhra Pradesh, India*

Matthias Posselt

*Helmholtz-Zentrum Dresden-Rossendorf,  
Bautzner Landstraße 400, 01328 Dresden, Germany*

Assa Aravindh Sasikala Devi

*Nano and molecular systems research unit, P.O.Box 8000,  
FI-90014, University of Oulu, Oulu, Finland*

(Dated: December 7, 2021)

# Abstract

The quasiparticle electronic structure and optical excitation of anatase  $\text{TiO}_2$  is determined within the framework of many-body perturbation theory (MBPT) by combining the  $G_0W_0$  method and the Bethe-Salpeter Equation (BSE). A modified version of the HSE06 screened hybrid functional, that includes 20% exact Fock exchange (HSE06(20)) as opposed to 25% in the standard HSE06 functional, is used to set up the starting Hamiltonian for  $G_0W_0$ +BSE calculations. The HSE06(20) functional accurately predicts the ground state electronic band structure. BSE calculations based on data from  $G_0W_0$ +HSE06(20) yield direct optical excitation energies and oscillator strengths in excellent agreement with existing experiments and theoretical calculations characterizing direct excitation. In particular, an exciton binding energy of  $229 \pm 10$  meV is obtained, in close agreement with experiments. The projections of excitonic states onto the quasiparticle band structure in a fatband representation shows that the lowest optical transition of anatase  $\text{TiO}_2$  consists of excitons originating from the mixing of direct transitions within band pairs running parallel to the  $\Gamma - Z$  direction in the tetragonal Brillouin zone. This implies a strong spatial localization of excitons in the  $xy$  plane of the lattice. This investigation highlights the importance of a suitable non-interacting Hamiltonian for the MBPT based quasiparticle  $G_0W_0$  and subsequent BSE calculations and suggests HSE06(20) as an optimal choice in the case of anatase  $\text{TiO}_2$ .

## I. INTRODUCTION

In the ever growing arena of renewable energy and photo-catalysis, Titanium Dioxide ( $\text{TiO}_2$ ) is one of the most widely explored metal-oxides owing to its charge transport and oxidation properties along with its abundance, non-toxicity, and corrosion resistance.  $\text{TiO}_2$  finds promising applications in areas such as photo-generation of hydrogen from water[1–3], photo-active and opto-electronic devices[4, 5], dye-sensitized solar cells(DSSC)[4, 6–8], degradation of pollutants under visible-light irradiation[9, 10], production of hydrocarbon fuels[11, 12],

---

\* aloksharan@gmail.com

antimicrobial coatings[13], nonlinear optical applications[14] and so on. Among the naturally occurring TiO<sub>2</sub> polymorphs, the anatase form is generally regarded as the more active phase in photo-catalysis than its other polymorphs-rutile and brookite[15–18]. Thin films of anatase has a wider optical-absorption gap and smaller electron effective mass that presumably leads to its higher charge carrier mobility[6, 19]. Anatase TiO<sub>2</sub> plays a key role in the injection process of photo-chemical solar cells with high conversion efficiency[4–7]. Tailor-made applications of these physico-chemical properties[20] can be achieved by tuning the photoresponse by doping with noble gas[21], various metals[13, 22–25] as well as by strain engineering[26, 27].

Rigorous approaches that goes beyond mean-field theory are necessary to quantitatively model photoemission and optical absorption in pristine anatase TiO<sub>2</sub>[22, 28–32]. The important physical quantities which are related to electrical and optical excitation in anatase TiO<sub>2</sub> are accurately determined computationally within the many-body perturbation theory (MBPT)[33–35]. Within the MBPT framework, the *GW* approximation (GWA)[33, 36–46] is commonly used for calculating quasiparticle energies and the Bethe-Salpeter equation (BSE) to include excitonic effects[47–49]. *GW* method in combination with the Bethe-Salpeter equation (BSE)[47, 48] represents a standard many-body approach for the accurate determination of the band structure and optical properties of semiconductors [33]. The simplest and most efficient computational implementation of *GW* is the single-shot-*GW*, often referred to as  $G_0W_0$ [50–56]. In  $G_0W_0$  method, quasiparticle eigenvalues are estimated from a single *GW* iteration, by perturbative Taylor expansion of self-energy around the DFT single-particle energies[39, 41, 57–59]. Although  $G_0W_0$  is proven to be accurate enough for determining eigen energies, bandgaps, bandwidths, and band dispersion for semiconductors[39, 41, 58, 59] the lack of self-consistency in  $G_0W_0$  makes its extremely sensitive to the DFT initial wavefunction. Hence this choice has to be made carefully in order to capture the "right" amount of electronic screening[60, 61].

Compared to LDA/GGA[62–64] or DFT+U[65], DFT wavefunction with hybrid exchange and correlation(XC) functionals[66–68] are widely regarded as the most reasonable starting point for  $G_0W_0$  calculations[47, 69–74]. Hybrid function-

als formally describe non-local two-particle scattering processes explicitly[75, 76], and therefore, the resulting wavefunction are already close to the quasiparticle wavefunction. It remedies the bandgap underestimation by LDA/GGA functionals[62–64, 77–88]. With regards to TiO<sub>2</sub> polymorphs, hybrid functionals do not cause lattice distortions[89, 90], which is otherwise one of the shortcomings of DFT+U when sub-optimal U values are used[89–91]. As far as Ti-3d states in anatase TiO<sub>2</sub> and other 3d transition-metal compounds are concerned, it is important that the starting wavefunction must describe its localized character and true nature of bonding[92–99]. In comparison to LDA/GGA and DFT+U[65] methods, hybrid functionals reproduce the correct bandgap, localization of orbitals, ordering and occupation of bands leading to much meaningful quasiparticle properties and dielectric functions[47, 69, 73, 100, 101].

To date, optical properties of pristine anatase TiO<sub>2</sub> taking the effect of many-body interactions into account have been addressed only by few computational studies[28–31, 102]. Majority of these studies rely on GGA(PBE) DFT wavefunction as starting point. To the best of our knowledge, apart from a recent study by Basera *et al.*[100], there has been no theoretical study of the optical response of pristine anatase TiO<sub>2</sub> exploring the role of hybrid functionals starting points in the MBPT calculations. In most of these studies, however, incongruous comparison of direct optical gap of TiO<sub>2</sub> obtained by solving BSE is made with indirect optical gap, and binding energy of excitons are underestimated.

We investigate the use of hybrid DFT wavefunction as starting point of MBPT calculations of quasiparticle excitation and excitonic optical spectra of pristine anatase TiO<sub>2</sub>. HSE06 screened hybrid functional[66, 103] DFT Hamiltonian has been employed as the starting point for MBPT calculations. Single particle excitation are calculated by  $G_0W_0$  and excitonic effects in the optical response of anatase TiO<sub>2</sub> are treated within the BSE framework. Standard recipes of hybrid functionals prescribe the portion of exact exchange( $\alpha$ ) to be fixed independent of the system being investigated. However, in general,  $\alpha$  is material dependent[104–108] and is related to dielectric screening of the material[109]. As we show in the present work, the optical response of anatase TiO<sub>2</sub> is extremely tunable by adjusting the internal parameters of Hybrid functionals. In search of the best

hybrid functional wavefunction for MBPT calculation, we optimize the fraction of exact exchange in the HSE06 functional in such a way that the modified functional correctly predicts both the ground state electronic structure and excited state response of pristine anatase  $\text{TiO}_2$ . The results of MBPT calculation with the proposed modified HSE06 functional is then discussed and compared with the existing literature. This study will act as a reliable benchmark of MBPT calculation for  $\text{TiO}_2$  and its possible extension at the same level of theory for all future calculations. Our investigation can benefit description of optical excitation of defective structures for which hybrid functionals are regularly employed [28, 100].

The article is organized as follows. The general methodologies and computational schemes for DFT and MBPT calculations are summarized in Sec. II. Sec. III presents results of optimization of DFT electronic structure (Sec. III A), Quasiparticle correction (Sec. III B) and excitonic optical spectra (Sec. III C) computed with our proposed modified HSE06 hybrids as starting points. Key approximations used in the study and numerical details pertaining to the calculation has also been discussed wherever necessary. We conclude the article in Sec. IV with a short discussion of our results, along with its limitations including the neglect of role of coupling of electronic excitation to phonons.

## II. METHODOLOGY AND COMPUTATIONAL DETAILS

Density functional theory (DFT) calculations employing hybrid functional are combined with methods based on many-body perturbation theory (MBPT). All ground state DFT,  $GW$ , and BSE calculations are performed using the Vienna ab-initio simulation package (VASP) [110–113]. Recommended PAW potentials[114, 115] supplied by VASP were employed for all atoms to describe the core-valence interactions. These PAW potentials are optimized for  $GW$ , as opposed to standard PAW potentials, and provide accurate description of scattering properties even at higher energies[57]. Besides the Ti ( $4s$  &  $3d$ ) and O ( $2s$  &  $2p$ ) valence states, the shallow Ti ( $3s$  and  $3p$ ) core states are also treated as valence electrons. Their inclusion is essential for accurate calculation of quasiparticle energy gaps[29],

the omission of which is shown to increase the quasiparticle bandgap as high as 0.3 eV[116]. Gaussian smearing with  $\sigma = 0.05$  eV was used to broaden the one electron levels. Based on the convergence of total free energy, we have set 520 eV as kinetic energy cut-off to describe the plane waves included in the basis set. An un-shifted  $\Gamma$ -centered  $6 \times 6 \times 3$  Monkhorst-Pack grid [117] is used for sampling the body-centered tetragonal Brillouin zone of anatase  $\text{TiO}_2$ . Initially, geometry of the conventional unit cell of bulk anatase  $\text{TiO}_2$  is relaxed by using the GGA (PBE) functional. During geometry relaxation, the volume, cell shape, and ions were allowed to relax until the force and energy becomes less than  $10^{-5}$  eV/Å and  $10^{-6}$  eV per atom, respectively. The relaxed tetragonal lattice is characterized by lattice constants:  $a = 3.805$  Å and  $c = 9.781$  Å, which are in reasonable agreement with lattice parameters measured in experiments[118–120].

The electronic structure of optimized anatase  $\text{TiO}_2$  is then calculated by introducing non-local part of the exchange as in hybrid density functionals [66–68]. In this work HSE06 screened hybrid functional as parametrized by Heyd-Scuseria-Ernzerhof [66, 68, 103, 121–123] and its modifications are used to represent the exchange correlation interactions. Screened hybrid functionals yields an accuracy in par with standard(full-range) hybrids[124–130] but with reduced computational cost[123, 131–135]. When applied to solids, screened hybrids has demonstrated tremendous success in predicting the band gaps of semiconductors and insulators[136, 137] with significantly smaller errors than pure density functional theory (DFT) calculations[67, 123, 132–135].

While designing a hybrid functional, the choice of mixing fraction( $\alpha$ ) is crucial to the bonding character, ordering and alignment of bands, and thus in the electronic and dielectric properties of the material. At an operational level, the parameters that define the screened hybrid functional form a two dimensional space spanned by the range separation parameter(screening parameter ( $\omega$ ) and the fraction of Fock exchange ( $\alpha$ )[129]. Given the variety of systems, there is no fixed, universal combination of these parameters ( $\omega, \alpha$ ) that leads to predictions with satisfying accuracy. Mixing fraction is often fixed based on the dielectric constant of the materials[108, 138, 139] following the interpretation of dielectric constant as inverse screening[131]. Based on fitting a large number of molecular

species to atomization energies the fraction of Fock exchange  $\alpha$  and the screening parameter  $\omega$  were originally set to 0.25 (25%) and  $0.2 \text{ \AA}^{-1}$ , respectively, for standard HSE06 functional[140, 141]. In the present investigation, we maintain the screening parameter at  $\omega = 0.20$ (corresponding to a screening length  $r_s = 2/\omega = 10 \text{ \AA}$ ). However, in the spirit of Ref. [128], Ref. [142] and Ref. [143]  $\alpha$  is tuned and optimized such that modified HSE06 functional yield a DFT bandgap close to experimental gap. The DFT wavefunction of modified HSE06 functional so obtained with the optimized  $\alpha$  is chosen as initial state for MBPT( $G_0W_0$ +BSE) calculations.

In the single-shot  $G_0W_0$  approximation, the orbitals  $|nk\rangle$  of well converged ground state DFT with HSE06 exchange-correlation functional is used to compute QP energies  $E_{QP}^{nk}$  as first order corrections. Optical properties were calculated by solving BSE for two particle-Green's functions whose kernel includes local field effects as well as screened electron-hole interaction[33, 49, 144]. In most cases it is sufficient to solve BSE in Tamm-Dancoff approximation[145–147] and corresponding VASP implementation has been made use of in our work. In the BSE routine as implemented in VASP, the screened exchange calculated in preceding  $G_0W_0$  calculation are used to approximate the electron-hole ladder diagrams[47, 52, 57, 148]. From the solution of the BSE the dielectric function of anatase  $\text{TiO}_2$  and oscillator strengths of optical transitions for incident polarization parallel and perpendicular to the crystallographic  $c$  axis is computed. Further, the excitation mechanism is explained by examining the exciton amplitude projections on the quasiparticle bandstructure[149, 150]. Based on the analysis, properties such as the nature of photo-generated charge carriers, their origin, spatial localization in the anatase  $\text{TiO}_2$  are also presented.

### III. RESULTS AND DISCUSSION

#### A. Optimization of HES06-DFT electronic structure

The search for optimal DFT wavefunction with HSE06 functional is carried out by varying the fraction of exact exchange ( $\alpha$ ) from 15% to 35% with an inter-

val of 5%. This range of  $\alpha$  for hybrid functionals has been shown to yield very good results for large class of systems[107, 109, 143, 151]. HSE06 ground state corresponding to each  $\alpha$  is henceforth referred to as HSE06( $\alpha$ ). For each  $\alpha$  the convergence of HSE06 bandgap is ensured by testing the convergence on 4 different k-point sets. The details of convergence study is presented in the figure 1. As is evident from the figure 1, in spite of the change in the density of kpoint sampling HSE06 gaps are seen to be converged to within 0.05 eV. Hence kpoint set for all further calculations has been fixed to a  $6 \times 6 \times 3$  grid. Typically, this density of kpoint sampling is more than sufficient to accurately represent the screened exchange interaction in metals and semiconductors, where as, dealing with bare exchange requires at least a  $(12 \times 12 \times 12)$  grid[123]. This demonstrates the computational efficiency one can achieve when screened hybrid exchange functionals are being used. For  $6 \times 6 \times 3$  the band gap increases from 3.04 eV to 4.36 eV as the fraction of exchange is increased from 15% through 35%. This apparent widening of HSE06 gaps in linear proportion to the increase in  $\alpha$  ( $\approx 3$  eV for every 5% increase in  $\alpha$ ) is consistent with the trend observed for hybrid functionals elsewhere[109, 142, 143, 152].

The best converged result for the HSE06( $\alpha$ ) band gap, compared to experimental reports (3.2 eV), is obtained for 20% exact exchange fraction with  $6 \times 6 \times 3$  grid sampling the Brillouin zone, which is  $3.34 \pm 0.05$  eV. This setting is maintained for the rest of the calculations, more importantly for optics calculations, as it reproduces the correct bandgap and band dispersion in anatase TiO<sub>2</sub>. For the rest of the manuscript we would use the notation HSE06(20) to represent the modified HSE06 functional with  $\alpha = 20\%$  in order to distinguish it from the standard HSE06 functional.

Fig. 2 presents the DFT bandstructure and the density of states of anatase TiO<sub>2</sub> computed using the HSE06(20) functionals along the high symmetric directions in the irreducible Brillouin zone of TiO<sub>2</sub>. For comparison, bandstructure obtained with local/semi-local GGA(PBE) functionals is also superposed in the figure 2. It is interesting to note that the dispersion of conduction and valence bands near the respective band edges remain similar under both GGA and HSE06(20) functional description[153]. The role of HSE06(20) functional on eigenvalues



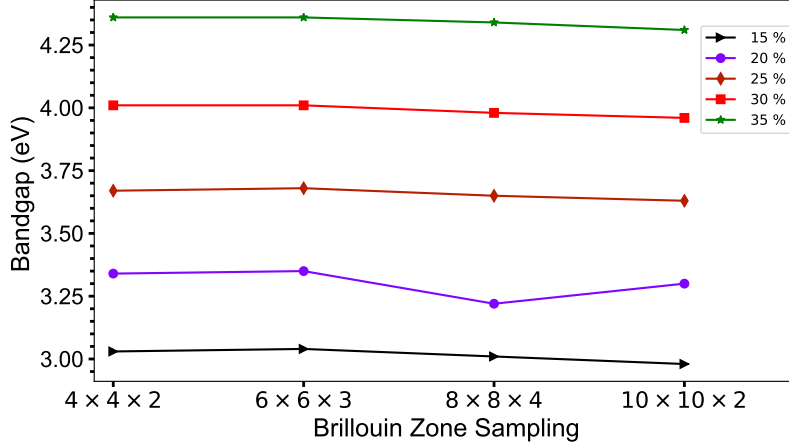


FIG. 1. The convergence of HSE06 bandgap for various values of exchange fraction ( $\alpha$ ) with respect to Brillouin zone sampling size. Each curve correspond to  $\alpha$  values from 15% to 35% with an interval of 5%. The HSE06( $\alpha$ ) gap is well converged to within 0.05 eV with respect to Brillouin zone sampling. For  $6 \times 6 \times 3$  kpoint grid, as  $\alpha$  increases band gap also increases at an approximate rate of 3 eV per 5% increase in the  $\alpha$ , which is represented quantitatively by a straight line  $E_g(\text{eV}) = 0.066\alpha(\%) + 2.038$ . The intercept of the fitted straight line closely matches the PBE band gap(2.11 eV). Due to the relative closeness of HSE06(20) gap to the experimental result, HSE06(20) wavefunction is chosen as zero order starting point for many-body perturbation theory calculations

appear nearly like a rigid upward shift of conduction bands, almost uniformly across all the bands and kpoints, from PBE counterparts. With the application of HSE06(20) functionals, the conduction band opens up by 1.23 eV, while the valence band remains unaffected. With conduction bands shifting up, the overall fundamental gap of pristine anatase  $\text{TiO}_2$  opens up to 3.34 eV. The computed bandgap is indirect with CBM at  $\Gamma$  point and VBM at  $0.91\Gamma \rightarrow M[143, 154]$ , consistent with the literature [28, 30, 155]. We observe that, the HSE06(20) DFT, in general, predicts bandgap which is more consistent with experimental data than LDA/GGA(PBE) functionals.

Compared to HSE06(20), standard HSE06(with  $\alpha = 0.25$ ) yields the fundamental gap at 3.68 eV in our calculation, which is overestimated. Similar overestimation tendencies have also been shown by other studies on  $\text{TiO}_2$  utilizing standard

hybrid functionals; which are 3.60 [30, 156], 3.57[157], 3.58[158], 3.59[108], 3.60[159], and 3.89 eV[93]. Another study bench-marking the performance of various functionals on large class of transition metal oxides and dichalcogenides reports a gap of 3.38 eV with standard HSE06 functional[160]. As a measure to remedy the overestimation of bandgap of TiO<sub>2</sub> by standard hybrid functionals, modified  $\alpha$  has as well been tested in extant studies. 20% exchange fraction in the HSE06 functional has been tested earlier for anatase TiO<sub>2</sub> by Janotti *et al.*. They obtain a bandgap of 3.05 eV, which is slightly underestimated[161]. In another study, Çelik and Mete found an indirect bandgap of 3.20 eV in the  $X - \Gamma$  direction by employing HSE functional with a mixing fraction of 0.22[151].

HSE06(20) density of states of anatase TiO<sub>2</sub> shown in figure 3 and the fatband representation of O-2*p* and Ti-3*d* orbitals projected on to the PBE bandstructure (figure 2, right panel) reveals that the top region of the valence band is occupied by O-*p* orbitals. Conduction bands populated primarily by the Ti-3*d* like orbitals, shows a splitting mainly into two groups, one lying above and one below 4.5 eV. This splitting is a result of lifting of the degeneracy of Ti-3*d* orbitals due to the distortion of TiO<sub>6</sub> octahedra, typical to anatase[162, 163]. The coordination of Oxygen ions around Titanium ions form a distorted octahedral crystal field inducing splitting of Ti-3*d* orbitals into triply degenerate  $t_{2g}$  (states below 4.5 eV) and doubly degenerate  $e_g$  (states above 4.5 eV)[30, 162–164]. The density of states shown in Ref. [165] reveals that the joint contribution of Ti-3*d* and O-2*p* orbitals near the band edges, coupled with strong dispersion of bands is an indication of hybridization of O-2*p* and Ti-3*d* orbitals. Hybridization of orbitals in the vicinity of Fermi level leads to the formation of covalent Ti-O bonds[163, 166, 167]. Covalent nature of the bonds has been established also by determining the charge enclosed within the Bader charge volume[168] of respective ions. From the Bader charge analysis we arrive at Bader-charge based ionic charge states of Ti<sup>2.26+</sup> and O<sup>1.12-</sup>. The departure of ionic charge states from the expected nominal ionic valences of +4 and -2 for Ti and O, respectively, is an indication of strong covalent character of the Ti–O bond. It has been established here that the involvement of *d* orbitals in the electronic structure of TiO<sub>2</sub> brings about a significant degree of covalent character and distortion of otherwise atom-like charge surrounding the

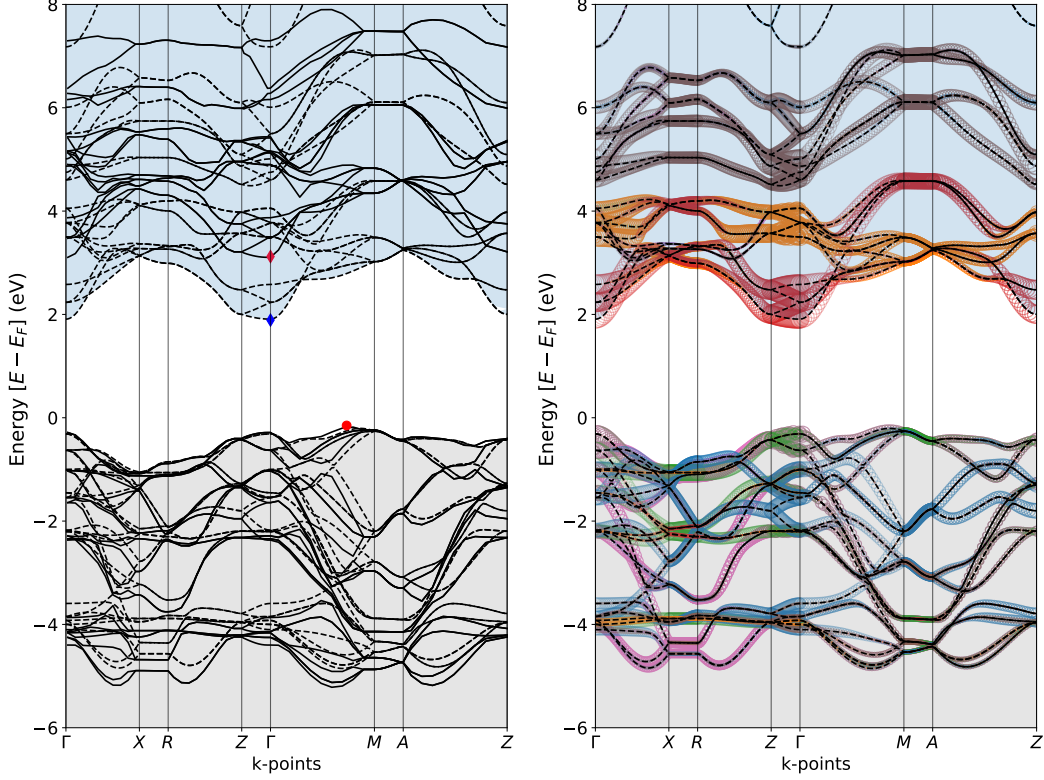


FIG. 2. The HSE06(20) and GGA(PBE) band structure calculated along the  $\Gamma - X - R - Z - \Gamma - M - A - Z$  high symmetric directions in the irreducible Brillouin zone (IBZ) of anatase  $\text{TiO}_2$ . Dotted and solid black lines represent the PBE and HSE06(20) bands, respectively. The energy reference is taken to be the Fermi energy. In the left panel, the red and blue diamonds label the conduction band minimum as obtained in HSE06(20) and GGA(PBE) bandstructure, respectively. The red circle labels the valence band maximum, which is the same with both GGA and HSE06(20). The value of bandgap as obtained with HSE06(20) and GGA(PBE) are both indirect, which are 3.34 eV and 2.11 eV, respectively. Bands are generally dispersive indicating at all regions of the Brillouin zone showing the covalent nature of bonding between Ti and O ions. In the right panel, O-2p and Ti-3d orbitals are projected onto the PBE bandstructure in a fatband form. In the figure circles projected on the bands represent O- $p_x$  (pink),  $p_y$  (green),  $p_z$  (blue) and Ti- $d_{xy}$  (red),  $d_{yz}$  (orange),  $d_{xz}$  (gray),  $d - t_{2g}$  (brown) orbital contributions to the bandstructure. Topmost valence band and lowest conduction band, which are nearly parallel along the  $\Gamma - Z$  direction, provide joint density for intense optical transitions between O- $p_x$  and  $p_y$  states in the valence band to Ti- $d_{xy}$  in the conduction band.

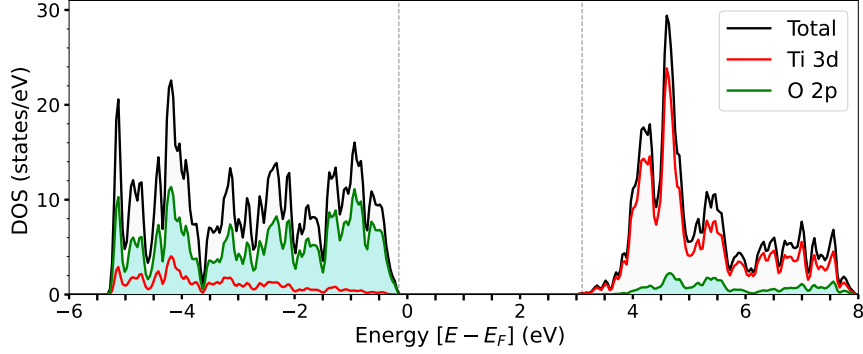


FIG. 3. The total and atom projected-angular momentum decomposed density of states showing the Ti-3d and O-2p contributions to the local density of states: Energies in DOS are reported with reference by setting Fermi energy as zero. In the DOS, valence bands and conduction bands predominantly composed of O-2p and Ti-3d states respectively. However, there are hybridization of Ti-3d and O-2p orbitals in both the regions. Ti 3d states in the conduction band region is split into two regions, lying above and below 4.5 eV, as a result of degeneracy of Ti-3d orbitals being lifted due to the distorted  $\text{TiO}_6$  octahedra. States below 4.5 eV constitute the  $t_{2g}$  states and those above form  $e_g$  based on the crystal field splitting induced by the distorted octahedral coordination of Oxygen ions around Ti.

Ti ion. As it is evident from the preceding discussion that, HSE06(20) very accurately reproduces the character of density of states as has been predicted in the literature[30, 162, 163]. We, by this analysis, have demonstrated that HSE06(20) functional captures the effect of Ti-3d electrons in the electronic structure, making it a good starting point for  $G_0W_0$  and BSE calculations for  $\text{TiO}_2$  anatase.

### B. $G_0W_0$ Quasiparticle corrections

The quasiparticle(QP) electronic structure is determined within the framework of MBPT using the single-shot  $G_0W_0$  approximation.  $G_0W_0$  QP corrections are computed on DFT eigenvalues obtained with HSE06(20) functionals(referred to as  $G_0W_0$ -HSE06(20)). In order to justify the comparison of  $G_0W_0$  electronic structure with the experimental outcomes, it is imperative to ensure that the calculation is well converged[29, 52, 57, 169, 170]. We carefully examine the convergence of

the  $G_0W_0$  calculations with respect to the number of empty states(virtual orbitals) and number of frequency points in the real space for the response functions. For all the convergence studies, the target quantity is the bandgap which is known to converge much faster than the absolute quasiparticle energies due to cancellation effects[29]. The cut-off for basis set for  $G_0W_0$  response function is set at rather conservative value of 150 eV for all calculations performed. The details of the convergence study is summarized in figure 4. Also shown in the figure 4 is a comparison of convergence behavior when PBE and HSE06(20) wavefunctions are used as initial wavefunction for  $G_0W_0$  QP corrections. Within the range of values of convergence parameters used in this work, QP gaps as well as HOMO and LUMO energies show similar rate of convergence irrespective of the starting wavefunction. Quasiparticle band gap is converged to within 0.01 eV when 256 bands (48 occupied and 208 virtual orbital), 100 points on the frequency grid and a  $6 \times 6 \times 3$  gamma centered kpoint grid are used. For even better convergence, one has to use larger energy cut-off, denser kpoint sampling and more number of empty states which would make the calculation practically not feasible due to forbidding memory requirements[171].

Our best converged  $G_0W_0$  quasiparticle calculation on top of modified HSE06 (20) wavefunction predicts a quasiparticle (QP) gap of 4.10 eV(indirect)/4.14 eV(direct) for pristine anatase  $\text{TiO}_2$ . This value is in reasonable agreement with prior studies that report  $G_0W_0$  QP gap obtained over hybrid functional starting points. Two of the most important contributions in this direction are by Kang and Hybertsen[29] and Landmann *et al.*[30], and both predicted band gap of 4.05 eV with HSE06+ $G_0W_0$  and HSE+ $G_0W_0$ , respectively. Rest of the  $G_0W_0$  calculations on  $\text{TiO}_2$  are performed on top of GGA or GGA+U DFT wavefunction starting points, and the most important results are compiled in Table I. As it is evident from the Table I,  $G_0W_0$  QP gaps computed with GGA and GGA+U DFT wavefunction starting points lie within the range from 3.3 to 3.92 eV and they are all lower than the QP gaps obtained on hybrid starting points[28–30, 172, 173]. The huge variability of  $G_0W_0$  QP gaps in the table I shows the poor consensus in the literature regarding the calculated QP bandgap of anatase  $\text{TiO}_2$ , revealing its strong sensitivity to computational setting and initial structural geometries.

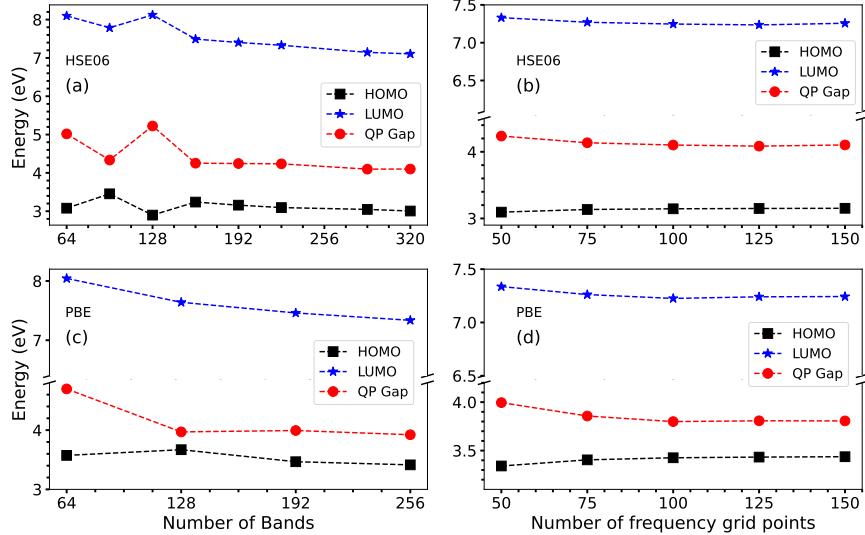


FIG. 4. Convergence of  $G_0W_0$  HOMO and LUMO energies, and bandgaps with respect to number of bands and number of frequency grid points for PBE and HSE06(20) starting wavefunction. Convergence of QP gap is faster compared to absolute HOMO and LUMO energies. QP gaps reported in this article is well converged to within 0.01 eV. Further, the convergence of absolute energies and QP energies better than 0.01 eV would require even more number of bands and denser k-point sampling. Convergence is moderately similar for both GGA and HSE06 starting wavefunctions

Considering the tendencies of HSE06 functionals to overestimate the  $G_0W_0$  QP gap of anatase  $\text{TiO}_2$ , there seems to be no real advantage of performing  $G_0W_0$  over hybrids in terms of accuracy of QP gaps. However, it can be shown that  $G_0W_0$  calculation on top of HSE06 wavefunction captures quasiparticle nature of electronic excitation and excitonic character of optical excitation which the GGA or DFT+U starting points fail to do[30]. This is evident from the amount of QP correction we obtain over HSE06( $\alpha$ ) and PBE starting wavefunction. We obtain a  $G_0W_0$  QP correction with respect to DFT indirect gap (2.11 eV) of 1.69 eV for anatase  $\text{TiO}_2$  over PBE starting point wavefunction while the same over the HSE06(20) indirect bandgap(3.34 eV) amounts to 0.76 eV only. With HSE06(25) and HSE06(30) starting points, QP corrections are 0.49 eV and 0.24 eV, respectively, over corresponding HSE06( $\alpha$ ) bandgap (Table II). As the exchange fraction( $\alpha$ ) is increased the  $G_0W_0$  correction for calculations starting from respec-

TABLE I.  $G_0W_0$  Quasiparticle gap ( $E_{gap}^{G_0W_0}$ ) and BSE optical gaps ( $E_{gap}^{Opt}$ ) computed over LDA/GGA, GGA+U and various hybrid functional starting wavefunction reported so far in the literature. All energies are in eV. The symbols I and D in parenthesis of QP gaps denotes if the band gaps are indirect or direct, respectively.

Starting Point	$G_0W_0$ QP Gap		Optical Gap	
	$E_{gap}^{G_0W_0}$ (eV)	Ref.	$E_{gap}^{Opt}$ (eV)	Ref.
HSE06(20)	4.1(I)/4.14(D)	Present work	3.911	Present work
HSE06	4.05(I)	[116]	3.45	[100]
HSE06	3.89(I)	[157]		
HSE	4.05(I)	[30]		
	3.8(I)/3.838(D)	Present work	3.745	Present work
	3.56(I)/4.14(D)	[29]	3.57	[30]
	3.83(I)/4.29(D)	[28]	3.90	[28]
	3.73(I)/3.78(D)	[30]	3.76	[31]
LDA/GGA	3.73(I)	[108]	4.0	[29, 162]
	3.7(I)	[173]	4.5	[30]
	3.791(I)	[26]		
	3.61(I)/3.92(D)	[31]		
	3.92(I)	[172]		
	3.5(I)/3.8(D)	[174]		
GGA+U	3.27	[173]		

tive modified HSE06( $\alpha$ ) bandstructure tend to vanish. Increasing  $\alpha$  makes the functional better at capturing quasiparticle nature of the excitation, and remedies the self-energy problem of PBE functionals. However, this would lead to further overestimation of fundamental gap of anatase TiO<sub>2</sub>.

### C. Optical transitions

To identify the microscopic nature of the optical excitation, the dielectric function of pristine anatase  $\text{TiO}_2$  is evaluated by solving Bethe-Salpeter Equation(BSE). The  $W_0$  of the preceding  $G_0W_0$ -HSE06(20) calculation and a  $\Gamma$ -centered, un-shifted  $6 \times 6 \times 3$  kpoint grid has been employed in the BSE calculation. BSE with HSE06(20) hybrid exchange as used in this work is henceforth referred to as BSE- $G_0W_0$ -HSE06(20) in the rest of the paper. The dielectric function is evaluated at 100 frequency points on the real axis. 20 BSE eigenvalues for the incident light polarized parallel and perpendicular to the  $c$ -axis are computed in the BSE step. Optical transition energies and exciton binding energies are thoroughly converged, each to within 10 meV, by including sufficient number of occupied and virtual orbitals in the BSE calculation[175]. For the final results presented here, 8 highest occupied and 16 lowest empty bands of the  $G_0W_0$ -HSE06(20) bandstructure are considered for solving BSE.

The computed imaginary part of the dielectric function ( $\epsilon_2(\omega)$ ) of anatase  $\text{TiO}_2$  along with oscillator strengths of optical transition is presented in figure 5. Taking the anisotropy associated with the tetragonal symmetry of the anatase lattice into account we resolve the  $\epsilon_2(\omega)$  into two components-  $E \perp c$  which is the average over the  $x$  and  $y$  components, and the  $E \parallel c$ (the  $z$  component). The first peak of  $\epsilon_2$  occurs for the  $E \perp c$  component corresponds to the direct optical gap 3.911 eV. It lies below the related direct quasiparticle bandgap( $G_0W_0$ -HSE06(20)) of 4.14 eV, confirming that the first direct optical excitation in anatase  $\text{TiO}_2$  is dominated by bound excitons. All other excitation are resonant excitation. We compute the binding energy concerning peak at 3.911 eV, i. e., the difference between first direct optical transition and direct quasiparticle gap, to be  $229 \pm 10$  meV.

The exciton wavefunction can be expressed as an electron-hole product basis  $\phi' = \sum_{cvk} A_{vck}^S \phi_{ck} \phi_{vk}$ , where  $v$  and  $c$  are valence and conduction band states at the  $k$  point, and  $A_{vck}^S$  is the exciton amplitude with the corresponding excitation energy  $E_{exc}^S$ . In order to determine the region of the Brillouin zone important for the optical gap, the eigenstate corresponding to the first exciton ( $S = 3$ ) from the BSE is visualized as fatband in Figure 6 by plotting circles of radius  $|A_{vck}^3|$  onto the



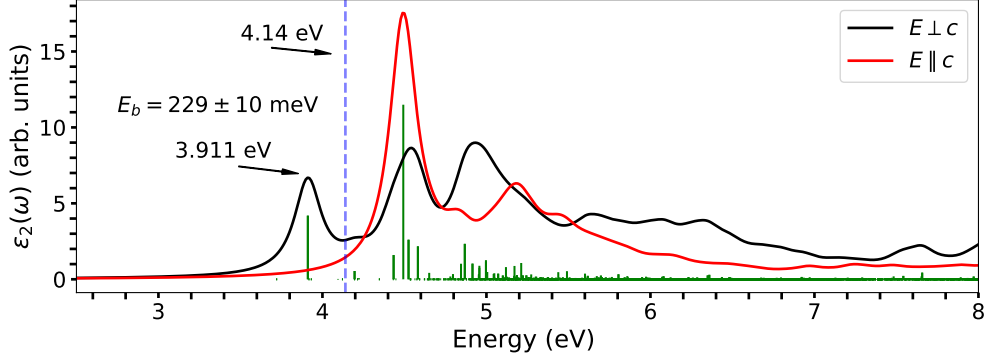


FIG. 5. The imaginary part of the dielectric function of anatase  $\text{TiO}_2$  computed within the BSE- $G_0W_0$ -HSE06(20) set up. In the figure, the optical response is shown for in-plane polarization ( $E \perp c$ ) and direction perpendicular to crystallographic  $c$  axis ( $E \parallel c$ ) by black and red solid curves, respectively. Green spikes in the figure represent the relative magnitude of oscillator strengths corresponding to optical transitions for both polarization. First peak in the dielectric function of anatase  $\text{TiO}_2$  is an excitonic peak. From the difference between first optical absorption obtained as solution to BSE and corresponding quasiparticle gap obtained in the  $G_0W_0$ -HSE06(20) calculation (blue, dashed vertical line at 4.10 eV) the exciton binding energy is estimated to be  $229 \pm 10$  meV .

bandstructure[149, 150, 176]. Black and green open squares in the fatband are BSE eigenvalues in the valence band and conduction band, respectively. Centered at the BSE hole(electron) eigenvalue in the valence band(conduction band) at a given  $k$  point, pairs of circles of identical colour represent an excitons which contribute most to the first excitonic peak in  $\epsilon_2$ . Only two highest occupied bands ( $v = 7, 8$ ) and two lowest unoccupied bands ( $c = 9, 10$ ) considered for BSE are important for the optical gap. The most important part of the Brillouin zone responsible for the excitonic peak in at 3.911 eV lies along the  $\Gamma - Z$  directions. To within the resolution of  $k$ -space available in our BSE calculation we can assert that other regions contribute only weakly. Previous BSE calculations have also arrived at a conclusion similar to the present study[28, 177]. Combining Figure 6 with the HSE06(20) bandstructure (figure 2), these bands are identified to be composed of O- $p_x, p_y$  and Ti- $d_{xy}$  orbitals at valence band and the conduction band, respectively. Dispersion of lowest conduction band and the highest valence

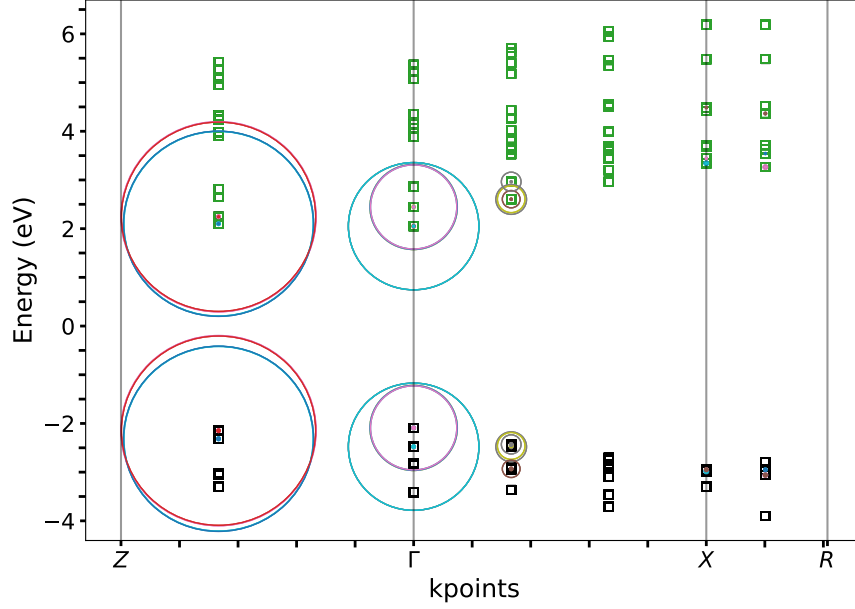


FIG. 6. The third BSE eigenvalues of electron-hole pairs (corresponding to first excitonic transition) of anatase  $\text{TiO}_2$  is visualized along with the strength coupling between them in fatband style. Black and green open squares in the fatband are BSE eigenvalues in the valence band and conduction band, respectively. Energies in the plot are shifted to make Fermi energy zero. The pairs of circles of same color and radii, one centered at a hole eigenvalue from the valence band and the other at an electron eigenvalue at the conduction band at a given  $k$ -vector represent an electron-hole pair. The radius of the circle is an indicative of relative coupling strength of individual exciton. The  $\Gamma$  and  $Z$  region of the Brillouin zone predominantly contribute to the first excitonic transitions while the rest of the regions contributes only weakly. This clearly shows the localization of excitons in the plane perpendicular to the  $c$ -axis of anatase unit cell.

band in the  $\Gamma - Z$  direction are nearly parallel, leading to similar electron and hole group velocities in this region. This provides a large joint density of states for the optical transitions providing stability and strong binding of excitons. Flatness of the bands in the  $\Gamma - Z$  direction indicates that orbital interactions in anatase  $\text{TiO}_2$  mainly run in the  $xy$  plane than in the  $z$  direction in the real space[178]. As excitonic states are also from the same region of the Brillouin zone, this immediately translate into localization of excitons on the  $xy$  plane in real space. Similar observation has been made by Ref. [179] and Ref. [31] wherein it is shown that

high degree of localization of bound exciton confine the excitons almost in a single atomic plane(in the  $xy$  plane). Besides, the localization of excitons predicted in this work with BSE- $G_0W_0$ -HSE06(20) agrees well with the analysis of spatial distribution of the exciton wavefunction in real space by Ref. [28] and Ref. [177].

Figure 7 summarizes the influence of fraction of Fock exchange ( $\alpha$ ) in the HSE06( $\alpha$ ) starting wavefunction on the prediction of optical response of anatase  $\text{TiO}_2$ . As it is evident from Figure 7, the oscillator strength of optical transitions remains unaffected as the percentage of Fock exchange is varied. Furthermore, the fatband representation of excitonic states in  $E \perp c$  direction for HSE06( $\alpha$ ) points to the fact that the Brillouin zone important for the first peak is still along the  $\Gamma - Z$  directions, irrespective of  $\alpha$ [180]. However, optical gaps and exciton binding energy is strongly affected by it. With HSE06(20) functional starting point we obtain an optical gap of 3.911 eV corresponding to an exciton binding energy of  $229 \pm 10$  meV for this excitation. When  $\alpha$  is increased further to 25 and 30 % optical gap (exciton binding energy) also shifts to higher energies, 3.949 eV ( $261 \pm 10$  meV) and 3.992 eV ( $298 \pm 10$  meV), respectively. With an increase in the amount of Fock exchange ( $\alpha$ ), the quasiparticle gap ( $G_0W_0$  bandgap) becomes wider (Table II). A larger electronic gap makes the electronic screening less efficient, and consequently the electron-hole interaction is less screened. Therefore, the electron-hole pairs in the interacting levels become more bound.

In comparison to HSE06( $\alpha$ ) starting point, BSE calculations with PBE wavefunction show that there is no noticeable difference in the oscillator strengths of transitions in this case as well[181]. This can be very well related to the similarity of DOS and orbital composition for bands lying close to the bandgap in both descriptions. Similarly, the region of the Brillouin zone relevant for first optical peak predicted by PBE and HSE06( $\alpha$ ) starting points are also identical[182]. On the other hand, due to self-energy and related bandgap problem, the binding energy of excitons for the first peak at 3.745 eV with PBE functional as the starting point is  $93 \pm 10$  meV[183].

At this point it is important to emphasize that the present BSE calculations are performed for a frozen lattice with no consideration given for electron-phonon interactions. The excitons described in our BSE calculation are screened by the

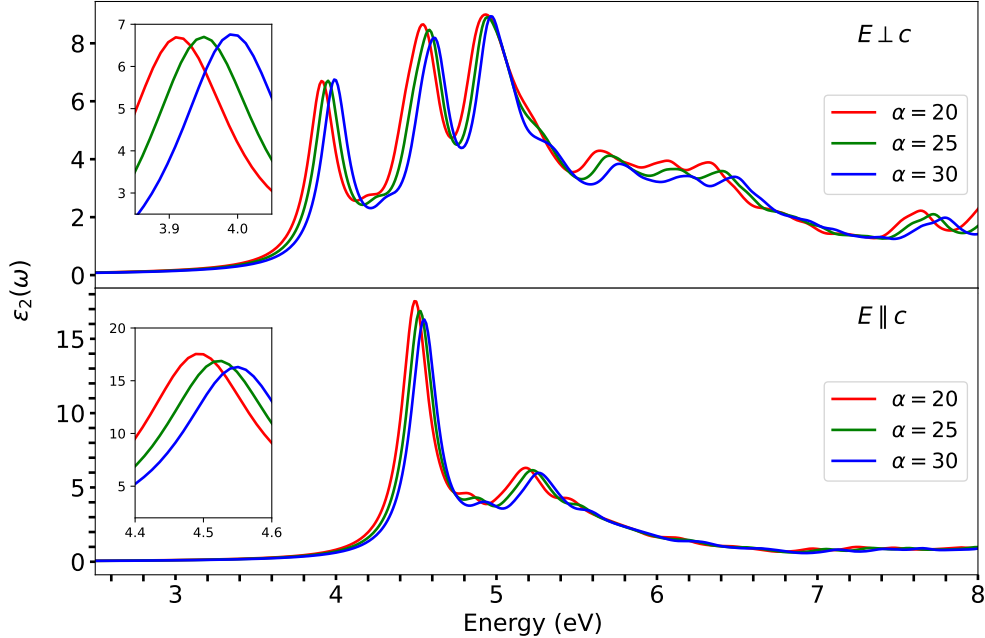


FIG. 7. Variation in the imaginary part of dielectric function of anatase  $\text{TiO}_2$  for in-plane and perpendicular polarization as a function of the fraction of Fock exchange ( $\alpha$ ) in the modified(HSE06) starting point for BSE calculation. The peak correspond to first direct optical transition is blue-shifted as the value of  $\alpha$  is increased. In a similar fashion, the excitons become more strongly bound as  $\alpha$  is increased.

electronic component alone. Ionic relaxation and lattice rearrangements induced by exciton formation[184] and the influence of intrinsic defects[93, 185] are not taken into account in our calculation. Hence the optical gap computed in our BSE calculations can only be compared with measured direct optical gaps (computational or experimental). In the case of pristine anatase  $\text{TiO}_2$ , as evidenced by the large difference between static and optical dielectric constants (static (optical) dielectric constants : 45.1(5.82) for  $E \perp c$  and 22.7(5.41) for  $E \parallel c$ ), the lattice relaxations has strong influence on the dynamics of excited charges[186]. Moreover, at finite temperatures, electron-phonon interactions and lattice thermal expansion affect temperature band gap renormalization in anatase  $\text{TiO}_2$ [187]. As a result, 3.2 eV, which is widely considered as the absorption edge of anatase  $\text{TiO}_2$  in several experimental investigations[188–191], is indeed due to indirect processes[19, 31, 162, 188, 192–196]. The allowed direct transitions have been

TABLE II. HSE06( $\alpha$ ) indirect gap ( $E_{HSE06}^I(\alpha)$ ), Indirect and direct quasiparticle gap ( $E_{QP}^I, E_{QP}^D$ ), quasiparticle correction over indirect bandgap ( $E_{QP}^I - E_{HSE06}^I(\alpha)$ ), BSE optical gaps ( $E_{Optical}^D$ ) and exciton binding energy of anatase TiO<sub>2</sub> as a function of Fock exchange fraction( $\alpha$ ) in the HSE06( $\alpha$ ) set-up.

$\alpha$ (%)	$E_{HSE06}^I(\alpha)$ (eV)	$E_{QP}^I$ (eV)	$E_{QP}^I - E_{HSE06}^I(\alpha)$ (eV)	$E_{QP}^D$ (eV)	$E_{Optical}^D$ (eV)	$EB$ (meV)
20	3.34	4.10	0.76	4.14	3.911	229
25	3.68	4.17	0.49	4.21	3.949	261
30	4.01	4.25	0.24	4.29	3.992	298

previously found by spectroscopic ellipsometry at 3.8 eV, and 3.79 eV, respectively, by Ref. [191] and Ref.[31] and at 3.87 eV by photoluminescence as in Ref. [197]. Our estimate of BSE direct optical gap of 3.911 eV computed over HSE06(20) starting wavefunction is in close agreement these experimental data for direct excitation.

Theoretical estimate of optical gaps by BSE calculations of pristine anatase TiO<sub>2</sub> lies in a wide range from 3.45 to 4.5 eV (Table I). Extant literature shows that the use hybrid functional as the starting wavefunction for BSE calculation of anatase TiO<sub>2</sub> is not very well explored. One such BSE study reported an optical gap of 3.45 eV[100] for  $E \perp c$  polarization using the standard HSE06 functional as starting wavefunction. This is the the lowest of all available BSE calculations of pristine anatase TiO<sub>2</sub>, and is underestimated compared to results obtained in present investigation. With PBE functional starting wavefunction, direct optical gap obtained from BSE calculation for anatase single crystals by Ref. [31](3.76 eV) yields excellent agreement with spectroscopic ellipsometric study (3.79 eV), making it the most reliable estimate of optical gap so far. In the present work, optical gap obtained with HSE06(20) starting point (3.911 eV) and that for PBE starting point (3.745 eV) are very similar to each other. Both of these values are closer to experimental value presented in Ref. [31] as well. However, because of the smaller bandgap, the exciton binding energy estimated with PBE starting point (93 meV) is much smaller than its HSE06(20) counterpart (229 meV). In

comparison to the value of exciton binding energy derived from experiments (180 meV) and also obtained consistently from frozen-atom BSE calculation (160 meV) in Ref. [31], prediction from HSE06(20) starting wavefunction is much closer. Experiments and frozen-atom BSE calculations reported in Ref. [31] are both performed at 20° C. According to Ref. [31], at 20° C, the combined effect of the temperature dependent lattice expansion and electron–phonon coupling is in fact negligible in pristine anatase TiO<sub>2</sub>.

#### IV. CONCLUSION AND OUTLOOK

To conclude, we systematically investigated the quasiparticle electronic structure and optical excitation of anatase TiO<sub>2</sub> within the framework of many-body perturbation theory (MBPT) by combining the  $G_0W_0$  method and the Bethe-Salpeter Equation (BSE). Non-interacting DFT Hamiltonian with a modified version of the HSE06 screened hybrid functional is employed as the starting point for  $G_0W_0 + \text{BSE}$  calculations. Fraction of exact Fock exchange in the HSE06 functional is tuned and the one which yields reasonably accurate ground state electronic structure is chosen as starting point for  $G_0W_0 + \text{BSE}$  simulations. Ground state DFT calculation with HSE06(20) functional yields 3.34 eV as the electronic gap of anatase TiO<sub>2</sub>. It reliably predicts the covalent character of Ti-O bonds, electronic bandstructure, fundamental gap and density of states of TiO<sub>2</sub>. Further, carefully converged  $G_0W_0 + \text{BSE}$  calculation on HSE06(20) starting wavefunction predicts first direct optical excitation of anatase TiO<sub>2</sub> at 3.911 eV, in agreement with experiments that measures direct optical excitation. This optical excitation creates strongly bound excitons with binding energy of  $229 \pm 10$  meV, with respect to  $G_0W_0$ -HSE06(20) quasiparticle gap. The projections of excitonic states onto the quasiparticle band structure in a fatband representation shows that the optical transition at 3.911 eV consists of excitons are originating from the mixing of single direct transitions within band pairs running parallel to the  $\Gamma - Z$  direction in the tetragonal Brillouin zone.

The present work highlights the importance of a suitable non-interacting Hamiltonian for the use in quasiparticle MBPT and subsequent BSE calcula-

tions. We observe that, irrespective of PBE or HSE06( $\alpha = 20, 25, 30\%$ ), the BSE excitonic spectra computed with respective starting points predicts the region of Brillouin zone important for optical gap to be along the  $\Gamma - Z$ . Nevertheless, as we obtained in the present work,  $G_0W_0 + \text{BSE}$  on PBE functional starting points underestimates the exciton binding energy( $93 \pm 10$  meV) of anatase  $\text{TiO}_2$ . The exciton binding energy as predicted in the present work with HSE06(20) starting wavefunction is more consistent with literature than those with LDA/GGA or DFT+U starting points. This leaves HSE06(20) as an optimal choice for non-interacting Hamiltonian for MBPT calculation in the case of anatase  $\text{TiO}_2$ .

Ground state (DFT) and excited state (MBPT) properties computed based on HSE06(20) functional are very encouraging for its continued use and extension into other systems too. This generalization is particularly true in the case of other metal and transition metal oxides where localized  $d$  and  $f$  electrons strongly influence the electronic structure and optical response. Our study provides a reference to MBPT calculation of doped  $\text{TiO}_2$  and with intrinsic defects so that reasonable comparison of physical observable at same level theory can be performed. This MBPT calculation of pristine anatase  $\text{TiO}_2$  with HSE06(20) functional starting point will serve as a benchmark for extending calculation into systems where we cannot exclude the significant role of exchange-correlations in starting wavefunction and  $d$  electron localization problem.

The prediction of strongly bound excitons in anatase  $\text{TiO}_2$  and its localization enabled by BSE calculation on HSE06(20) can potentially help us throw light on some of the challenging and open questions in the literature related to  $\text{TiO}_2$ . Characterizing band alignment in anatase and rutile structures with HSE06(20) functionals would deepen our insights on longstanding questions such as why anatase-rutile mixed phases[198, 199] are more photo-catalytically active than individual phases. Another challenge is related to the reactivity of different facets in anatase  $\text{TiO}_2$ . The particular spatial localization of excitons in the {001} plane can partly offer possible explanations to the question as to why the thermodynamically less stable {001} facets in  $\text{TiO}_2$  is more photo-reactive compared to stable {101} ones[200–203]. The advancement in controlled synthesis of anatase  $\text{TiO}_2$  having defined crystal facets at desired crystallographic

orientations[200, 204, 205], harvesting the exciton delocalization in anatase for devices, and nonlinear optical applications has become close to reality. The demonstration of selective and controlled modulation of oscillator strength of excitons by acoustic phonons[206] and huge exciton shifts by coupling exciton to the optically induced strain pulses[207] in anatase TiO<sub>2</sub> nanoparticles hold huge promises in this direction. For modelling such physical processes and design further experiments and devices, HSE06(20) hybrid functional based MBPT computations will definitely act as reliable benchmarks and test strategy.

- 
- [1] A. Fujishima and K. Honda, Electrochemical photolysis of water at a semiconductor electrode, *nature* **238**, 37 (1972).
  - [2] A. Fujishima, T. N. Rao, and D. A. Tryk, Titanium dioxide photocatalysis, *Journal of photochemistry and photobiology C: Photochemistry reviews* **1**, 1 (2000).
  - [3] A. Mills, N. Elliott, G. Hill, D. Fallis, J. R. Durrant, and R. L. Willis, Preparation and characterisation of novel thick sol-gel titania film photocatalysts, *Photochemical & Photobiological Sciences* **2**, 591 (2003).
  - [4] Y. Bai, I. Mora-Sero, F. De Angelis, J. Bisquert, and P. Wang, Titanium dioxide nanomaterials for photovoltaic applications, *Chemical reviews* **114**, 10095 (2014).
  - [5] S. Chen, M. Yu, W.-P. Han, X. Yan, Y.-C. Liu, J.-C. Zhang, H.-D. Zhang, G.-F. Yu, and Y.-Z. Long, Electrospun anatase tio 2 nanorods for flexible optoelectronic devices, *RSC advances* **4**, 46152 (2014).
  - [6] M. Grätzel, Solar energy conversion by dye-sensitized photovoltaic cells, *Inorganic chemistry* **44**, 6841 (2005).
  - [7] B. O'regan and M. Gratzel, A low-cost, high-efficiency solar cell based on dye-sensitized colloidal tio 2 films, *nature* **353**, 737 (1991).
  - [8] A. Hagfeldt and M. Grätzel, Molecular photovoltaics, *Accounts of Chemical Research* **33**, 269 (2000).
  - [9] T. L. Thompson and J. T. Yates, Surface science studies of the photoactivation of tio2 new photochemical processes, *Chemical reviews* **106**, 4428 (2006).
  - [10] X. Chen and S. S. Mao, Titanium dioxide nanomaterials: synthesis, properties,



- modifications, and applications, *Chemical reviews* **107**, 2891 (2007).
- [11] S. U. Khan, M. Al-Shahry, and W. B. Ingler, Efficient photochemical water splitting by a chemically modified n-tio<sub>2</sub>, *science* **297**, 2243 (2002).
- [12] O. K. Varghese, M. Paulose, T. J. LaTempa, and C. A. Grimes, High-rate solar photocatalytic conversion of co<sub>2</sub> and water vapor to hydrocarbon fuels, *Nano letters* **9**, 731 (2009).
- [13] A. M. Alotaibi, B. A. Williamson, S. Sathasivam, A. Kafizas, M. Alqahtani, C. Sotelo-Vazquez, J. Buckeridge, J. Wu, S. P. Nair, D. O. Scanlon, *et al.*, Enhanced photocatalytic and antibacterial ability of cu-doped anatase tio<sub>2</sub> thin films: theory and experiment, *ACS applied materials & interfaces* **12**, 15348 (2020).
- [14] N. Yaqub, W. Farooq, and M. AlSalhi, Nonlinear optical properties of lldpe composites with titanium dioxide anatase phase, *Journal of King Saud University-Science* , 101723 (2021).
- [15] M. Xu, Y. Gao, E. M. Moreno, M. Kunst, M. Muhler, Y. Wang, H. Idriss, and C. Woll, Photocatalytic activity of bulk tio<sub>2</sub> anatase and rutile single crystals using infrared absorption spectroscopy, *Physical Review Letters* **106**, 138302 (2011).
- [16] O. Carp, C. L. Huisman, and A. Reller, Photoinduced reactivity of titanium dioxide, *Progress in solid state chemistry* **32**, 33 (2004).
- [17] T. Luttrell, S. Halpegamage, J. Tao, A. Kramer, E. Sutter, and M. Batzill, Why is anatase a better photocatalyst than rutile?-model studies on epitaxial tio<sub>2</sub> films, *Scientific reports* **4**, 1 (2014).
- [18] T. Sumita, T. Yamaki, S. Yamamoto, and A. Miyashita, Photo-induced surface charge separation of highly oriented tio<sub>2</sub> anatase and rutile thin films, *Applied Surface Science* **200**, 21 (2002).
- [19] H. Tang, K. Prasad, R. Sanjines, P. Schmid, and F. Levy, Electrical and optical properties of tio<sub>2</sub> anatase thin films, *Journal of applied physics* **75**, 2042 (1994).
- [20] X. Kang, S. Liu, Z. Dai, Y. He, X. Song, and Z. Tan, Titanium dioxide: from engineering to applications, *Catalysts* **9**, 191 (2019).
- [21] M. Pelaez, N. T. Nolan, S. C. Pillai, M. K. Seery, P. Falaras, A. G. Kontos, P. S. Dunlop, J. W. Hamilton, J. A. Byrne, K. O'shea, *et al.*, A review on the visible light active titanium dioxide photocatalysts for environmental applications, *Applied*

- Catalysis B: Environmental **125**, 331 (2012).
- [22] M. O. Atambo, D. Varsano, A. Ferretti, S. S. Ataei, M. J. Caldas, E. Molinari, and A. Selloni, Electronic and optical properties of doped tio 2 by many-body perturbation theory, *Physical Review Materials* **3**, 045401 (2019).
- [23] J. Kulczyk-Malecka, P. Kelly, G. West, G. Clarke, J. Ridealgh, K. Almtoft, A. Greer, and Z. Barber, Investigation of silver diffusion in tio2/ag/tio2 coatings, *Acta materialia* **66**, 396 (2014).
- [24] Z. Li, J. Wu, D. Xiao, J. Zhu, and W. Wu, Colossal permittivity in titanium dioxide ceramics modified by tantalum and trivalent elements, *Acta Materialia* **103**, 243 (2016).
- [25] Z. Ma, F. Ren, Z. Yang, and A. A. Volinsky, Theoretical and experimental studies on electronic structure and optical properties of bi-doped anatase tio2, *Optik* **241**, 167107 (2021).
- [26] L. Thulin and J. Guerra, Calculations of strain-modified anatase tio2 band structures, *Physical Review B* **77**, 195112 (2008).
- [27] F. Maier, M. Schneider, J. Schratzenholzer, W. Artner, K. Hradil, A. Artemenko, A. Kromka, and U. Schmid, Flexoelectricity in polycrystalline tio2 thin films, *Acta Materialia* **190**, 124 (2020).
- [28] L. Chiodo, J. M. García-Lastra, A. Iacomino, S. Ossicini, J. Zhao, H. Petek, and A. Rubio, Self-energy and excitonic effects in the electronic and optical properties of tio 2 crystalline phases, *Physical Review B* **82**, 045207 (2010).
- [29] W. Kang and M. S. Hybertsen, Quasiparticle and optical properties of rutile and anatase tio 2, *Physical Review B* **82**, 085203 (2010).
- [30] M. Landmann, E. Rauls, and W. Schmidt, The electronic structure and optical response of rutile, anatase and brookite tio2, *Journal of physics: condensed matter* **24**, 195503 (2012).
- [31] E. Baldini, L. Chiodo, A. Dominguez, M. Palummo, S. Moser, M. Yazdi-Rizi, G. Auböck, B. P. Mallett, H. Berger, A. Magrez, *et al.*, Strongly bound excitons in anatase tio 2 single crystals and nanoparticles, *Nature communications* **8**, 1 (2017).
- [32] S. Tosoni, G. Di Liberto, and G. Pacchioni, Structural and electronic properties of

- tio<sub>2</sub> from first principles calculations, *Titanium Dioxide (TiO<sub>2</sub>) and Its Applications*, 67 (2020).
- [33] G. Onida, L. Reining, and A. Rubio, Electronic excitations: density-functional versus many-body green's-function approaches, *Reviews of Modern Physics* **74**, 601 (2002).
- [34] M. Rohlfing and S. G. Louie, Electron-hole excitations and optical spectra from first principles, *Physical Review B* **62**, 4927 (2000).
- [35] G. Strinati, Application of the green's functions method to the study of the optical properties of semiconductors, *La Rivista del Nuovo Cimento* (1978-1999) **11**, 1 (1988).
- [36] L. Hedin, New method for calculating the one-particle green's function with application to the electron-gas problem, *Physical Review* **139**, A796 (1965).
- [37] W. G. Aulbur, L. Jönsson, and J. W. Wilkins, Quasiparticle calculations in solids, *Solid state physics* (New York. 1955) **54**, 1 (2000).
- [38] F. Aryasetiawan and O. Gunnarsson, The gw method, *Reports on Progress in Physics* **61**, 237 (1998).
- [39] M. S. Hybertsen and S. G. Louie, First-principles theory of quasiparticles: calculation of band gaps in semiconductors and insulators, *Physical review letters* **55**, 1418 (1985).
- [40] R. Godby, M. Schlüter, and L. Sham, Accurate exchange-correlation potential for silicon and its discontinuity on addition of an electron, *Physical review letters* **56**, 2415 (1986).
- [41] M. S. Hybertsen and S. G. Louie, Electron correlation in semiconductors and insulators: Band gaps and quasiparticle energies, *Physical Review B* **34**, 5390 (1986).
- [42] R. Shaltaf, G.-M. Rignanese, X. Gonze, F. Giustino, and A. Pasquarello, Band offsets at the si/sio<sub>2</sub> interface from many-body perturbation theory, *Physical review letters* **100**, 186401 (2008).
- [43] M. J. van Setten, F. Weigend, and F. Evers, The gw-method for quantum chemistry applications: theory and implementation, *Journal of chemical theory and computation* **9**, 232 (2013).
- [44] H.-V. Nguyen, T. A. Pham, D. Rocca, and G. Galli, Improving accuracy and effi-

- ciency of calculations of photoemission spectra within the many-body perturbation theory, *Physical Review B* **85**, 081101 (2012).
- [45] P. Umari, G. Stenuit, and S. Baroni, Optimal representation of the polarization propagator for large-scale  $g w$  calculations, *Physical Review B* **79**, 201104 (2009).
- [46] P. Umari, G. Stenuit, and S. Baroni,  $Gw$  quasiparticle spectra from occupied states only, *Physical Review B* **81**, 115104 (2010).
- [47] F. Fuchs, J. Furthmüller, F. Bechstedt, M. Shishkin, and G. Kresse, Quasiparticle band structure based on a generalized kohn-sham scheme, *Physical Review B* **76**, 115109 (2007).
- [48] E. E. Salpeter and H. A. Bethe, A relativistic equation for bound-state problems, *Physical Review* **84**, 1232 (1951).
- [49] W. Hanke and L. J. Sham, Many-particle effects in the optical excitations of a semiconductor, *Phys. Rev. Lett.* **43**, 387 (1979).
- [50] C. Rostgaard, K. W. Jacobsen, and K. S. Thygesen, Fully self-consistent  $g w$  calculations for molecules, *Physical Review B* **81**, 085103 (2010).
- [51] F. Caruso, P. Rinke, X. Ren, M. Scheffler, and A. Rubio, Unified description of ground and excited states of finite systems: The self-consistent  $g w$  approach, *Physical Review B* **86**, 081102 (2012).
- [52] M. Shishkin and G. Kresse, Self-consistent  $g w$  calculations for semiconductors and insulators, *Physical Review B* **75**, 235102 (2007).
- [53] T. Kotani, M. van Schilfgaarde, and S. V. Faleev, Quasiparticle self-consistent  $g w$  method: A basis for the independent-particle approximation, *Physical Review B* **76**, 165106 (2007).
- [54] M. van Schilfgaarde, T. Kotani, and S. Faleev, Quasiparticle self-consistent  $g w$  theory, *Physical review letters* **96**, 226402 (2006).
- [55] B. Holm and U. von Barth, Fully self-consistent  $g w$  self-energy of the electron gas, *Physical Review B* **57**, 2108 (1998).
- [56] D. Tamme, R. Schepe, and K. Henneberger, Comment on “self-consistent calculations of quasiparticle states in metals and semiconductors”, *Physical review letters* **83**, 241 (1999).
- [57] M. Shishkin and G. Kresse, Implementation and performance of the frequency-

- dependent  $g$   $w$  method within the paw framework, *Physical Review B* **74**, 035101 (2006).
- [58] Á. Morales-García, R. Valero, and F. Illas, Performance of the  $g_0 w_0$  method in predicting the electronic gap of  $\text{TiO}_2$  nanoparticles, *Journal of chemical theory and computation* **13**, 3746 (2017).
- [59] F. Bechstedt, R. Del Sole, G. Cappellini, and L. Reining, An efficient method for calculating quasiparticle energies in semiconductors, *Solid state communications* **84**, 765 (1992).
- [60] T. Korzdorfer and N. Marom, Strategy for finding a reliable starting point for  $g_0 w_0$  demonstrated for molecules, *Physical Review B* **86**, 041110 (2012).
- [61] F. Bruneval and M. A. Marques, Benchmarking the starting points of the  $gw$  approximation for molecules, *Journal of chemical theory and computation* **9**, 324 (2013).
- [62] L. Sham and M. Schlüter, Density-functional theory of the band gap, *Physical Review B* **32**, 3883 (1985).
- [63] J. P. Perdew and A. Zunger, Self-interaction correction to density-functional approximations for many-electron systems, *Physical Review B* **23**, 5048 (1981).
- [64] J. P. Perdew, R. G. Parr, M. Levy, and J. L. Balduz Jr, Density-functional theory for fractional particle number: derivative discontinuities of the energy, *Physical Review Letters* **49**, 1691 (1982).
- [65] J. Hubbard, Electron correlations in narrow energy bands, *Proceedings of the Royal Society of London. Series A. Mathematical and Physical Sciences* **276**, 238 (1963).
- [66] J. Heyd, G. E. Scuseria, and M. Ernzerhof, Hybrid functionals based on a screened coulomb potential, *The Journal of chemical physics* **118**, 8207 (2003).
- [67] J. Heyd and G. E. Scuseria, Assessment and validation of a screened coulomb hybrid density functional, *The Journal of chemical physics* **120**, 7274 (2004).
- [68] A. V. Krukau, O. A. Vydrov, A. F. Izmaylov, and G. E. Scuseria, Influence of the exchange screening parameter on the performance of screened hybrid functionals, *The Journal of chemical physics* **125**, 224106 (2006).
- [69] F. Bechstedt, F. Fuchs, and G. Kresse, Ab-initio theory of semiconductor band structures: New developments and progress, *physica status solidi (b)* **246**, 1877

- (2009).
- [70] A. Schleife, J. Varley, F. Fuchs, C. Rodl, F. Bechstedt, P. Rinke, A. Janotti, and C. Van de Walle, Tin dioxide from first principles: Quasiparticle electronic states and optical properties, *Physical Review B* **83**, 035116 (2011).
- [71] C. Rodl, F. Fuchs, J. Furthmuller, and F. Bechstedt, Quasiparticle band structures of the antiferromagnetic transition-metal oxides mno, feo, coo, and nio, *Physical Review B* **79**, 235114 (2009).
- [72] F. Fuchs and F. Bechstedt, Indium-oxide polymorphs from first principles: Quasiparticle electronic states, *Physical Review B* **77**, 155107 (2008).
- [73] G. Cappellini, J. Furthmuller, E. Cadelano, and F. Bechstedt, Electronic and optical properties of cadmium fluoride: the role of many-body effects, *Physical Review B* **87**, 075203 (2013).
- [74] L. Y. Isseroff and E. A. Carter, Importance of reference hamiltonians containing exact exchange for accurate one-shot gw calculations of cu<sub>2</sub>o, *Physical Review B* **85**, 235142 (2012).
- [75] C. Friedrich, M. Betzinger, M. Schlipf, S. Blügel, and A. Schindlmayr, Hybrid functionals and gw approximation in the flapw method, *Journal of Physics: Condensed Matter* **24**, 293201 (2012).
- [76] J. Furthmüller, P. Hahn, F. Fuchs, and F. Bechstedt, Band structures and optical spectra of inn polymorphs: Influence of quasiparticle and excitonic effects, *Physical Review B* **72**, 205106 (2005).
- [77] J. P. Perdew, W. Yang, K. Burke, Z. Yang, E. K. Gross, M. Scheffler, G. E. Scuseria, T. M. Henderson, I. Y. Zhang, A. Ruzsinszky, *et al.*, Understanding band gaps of solids in generalized kohn-sham theory, *Proceedings of the National Academy of Sciences* **114**, 2801 (2017).
- [78] J. P. Perdew and M. Levy, Physical content of the exact kohn-sham orbital energies: band gaps and derivative discontinuities, *Physical Review Letters* **51**, 1884 (1983).
- [79] R. A. Heaton, J. G. Harrison, and C. C. Lin, Self-interaction correction for energy band calculations: Application to licl, *Solid State Communications* **41**, 827 (1982).
- [80] M. R. Norman and J. P. Perdew, Simplified self-interaction correction applied to the energy bands of neon and sodium chloride, *Physical Review B* **28**, 2135 (1983).

- [81] C. Wang and W. Pickett, Density-functional theory of excitation spectra of semi-conductors: application to si, *Physical review letters* **51**, 597 (1983).
- [82] O. A. Vydrov and G. E. Scuseria, Ionization potentials and electron affinities in the perdew–zunger self-interaction corrected density-functional theory, *The Journal of chemical physics* **122**, 184107 (2005).
- [83] O. A. Vydrov, G. E. Scuseria, J. P. Perdew, A. Ruzsinszky, and G. I. Csonka, Scaling down the perdew-zunger self-interaction correction in many-electron regions, *The Journal of chemical physics* **124**, 094108 (2006).
- [84] O. A. Vydrov and G. E. Scuseria, Effect of the perdew–zunger self-interaction correction on the thermochemical performance of approximate density functionals, *The Journal of chemical physics* **121**, 8187 (2004).
- [85] A. Seidl, A. Görling, P. Vogl, J. A. Majewski, and M. Levy, Generalized kohn-sham schemes and the band-gap problem, *Physical Review B* **53**, 3764 (1996).
- [86] A. J. Cohen, P. Mori-Sánchez, and W. Yang, Fractional charge perspective on the band gap in density-functional theory, *Physical Review B* **77**, 115123 (2008).
- [87] A. Ruzsinszky, J. P. Perdew, G. I. Csonka, O. A. Vydrov, and G. E. Scuseria, Spurious fractional charge on dissociated atoms: Pervasive and resilient self-interaction error of common density functionals, *The Journal of chemical physics* **125**, 194112 (2006).
- [88] M. Chan and G. Ceder, Efficient band gap prediction for solids, *Physical review letters* **105**, 196403 (2010).
- [89] V. I. Anisimov, F. Aryasetiawan, and A. Lichtenstein, First-principles calculations of the electronic structure and spectra of strongly correlated systems: the lda+ u method, *Journal of Physics: Condensed Matter* **9**, 767 (1997).
- [90] R. Gillen and J. Robertson, Accurate screened exchange band structures for the transition metal monoxides mno, feo, coo and nio, *Journal of Physics: Condensed Matter* **25**, 165502 (2013).
- [91] A. Raghav, A. T. Hanindriyo, K. Utimula, M. Abbasnejad, R. Maezono, and E. Panda, Intrinsic electronic defect states of anatase using density functional theory, *Computational Materials Science* **184**, 109925 (2020).
- [92] P. Mori-Sánchez, A. J. Cohen, and W. Yang, Localization and delocalization errors

- in density functional theory and implications for band-gap prediction, *Physical review letters* **100**, 146401 (2008).
- [93] G. Mattioli, P. Alippi, F. Filippone, R. Caminiti, and A. Amore Bonapasta, Deep versus shallow behavior of intrinsic defects in rutile and anatase tio<sub>2</sub> polymorphs, *The Journal of Physical Chemistry C* **114**, 21694 (2010).
- [94] H. Ünal, O. Gülseren, Ş. Ellialtıođlu, and E. Mete, Electronic structures and optical spectra of thin anatase tio<sub>2</sub> nanowires through hybrid density functional and quasiparticle calculations, *Physical Review B* **89**, 205127 (2014).
- [95] S. Na-Phattalung, M. F. Smith, K. Kim, M.-H. Du, S.-H. Wei, S. Zhang, and S. Limpijumnong, First-principles study of native defects in anatase ti o<sub>2</sub>, *Physical Review B* **73**, 125205 (2006).
- [96] M. Zhang, S. Ono, N. Nagatsuka, and K. Ohno, All-electron mixed basis g w calculations of tio<sub>2</sub> and zno crystals, *Physical Review B* **93**, 155116 (2016).
- [97] F. Aryasetiawan and O. Gunnarsson, Electronic structure of nio in the gw approximation, *Physical review letters* **74**, 3221 (1995).
- [98] S. V. Faleev, M. Van Schilfgaarde, and T. Kotani, All-electron self-consistent g w approximation: Application to si, mno, and nio, *Physical review letters* **93**, 126406 (2004).
- [99] F. Bruneval, N. Vast, L. Reining, M. Izquierdo, F. Sirotti, and N. Barrett, Exchange and correlation effects in electronic excitations of cu<sub>2</sub> o, *Physical review letters* **97**, 267601 (2006).
- [100] P. Basera, S. Saini, and S. Bhattacharya, Self energy and excitonic effect in (un)doped tio<sub>2</sub> anatase: a comparative study of hybrid dft, gw and bse to explore optical properties, *Journal of Materials Chemistry C* **7**, 14284 (2019).
- [101] P. Deak, Calculating the optical properties of defects and surfaces in wide band gap materials, *Physica B: Condensed Matter* **535**, 35 (2018).
- [102] T. Zhu and S.-P. Gao, The stability, electronic structure, and optical property of tio<sub>2</sub> polymorphs, *The Journal of Physical Chemistry C* **118**, 11385 (2014).
- [103] H. J. S. Ge and M. Ernzerhof, Erratum:“hybrid functionals based on a screened coulomb potential”[*j. chem. phys.* 118, 8207 (2003)], *J Chem Phys* **124**, 219906 (2006).



- [104] A. Alkauskas, P. Broqvist, F. Devynck, and A. Pasquarello, Band offsets at semiconductor-oxide interfaces from hybrid density-functional calculations, *Physical review letters* **101**, 106802 (2008).
- [105] A. Alkauskas, P. Broqvist, and A. Pasquarello, Defect levels through hybrid density functionals: Insights and applications, *physica status solidi (b)* **248**, 775 (2011).
- [106] A. Alkauskas, P. Broqvist, and A. Pasquarello, Defect energy levels in density functional calculations: Alignment and band gap problem, *Physical review letters* **101**, 046405 (2008).
- [107] I. de PR Moreira, F. Illas, and R. L. Martin, Effect of fock exchange on the electronic structure and magnetic coupling in nio, *Physical Review B* **65**, 155102 (2002).
- [108] M. Gerosa, C. E. Bottani, L. Caramella, G. Onida, C. Di Valentin, and G. Pacchioni, Electronic structure and phase stability of oxide semiconductors: Performance of dielectric-dependent hybrid functional dft, benchmarked against g w band structure calculations and experiments, *Physical Review B* **91**, 155201 (2015).
- [109] M. A. Marques, J. Vidal, M. J. Oliveira, L. Reining, and S. Botti, Density-based mixing parameter for hybrid functionals, *Physical Review B* **83**, 035119 (2011).
- [110] G. Kresse and J. Hafner, Ab initio molecular dynamics for open-shell transition metals, *Physical Review B* **48**, 13115 (1993).
- [111] J. Hafner, Ab-initio simulations of materials using vasp: Density-functional theory and beyond, *Journal of computational chemistry* **29**, 2044 (2008).
- [112] G. Kresse and J. Furthmüller, Efficient iterative schemes for ab initio total-energy calculations using a plane-wave basis set, *Physical review B* **54**, 11169 (1996).
- [113] G. Kresse and J. Furthmüller, Efficiency of ab-initio total energy calculations for metals and semiconductors using a plane-wave basis set, *Computational materials science* **6**, 15 (1996).
- [114] P. E. Blöchl, Projector augmented-wave method, *Physical review B* **50**, 17953 (1994).
- [115] G. Kresse and D. Joubert, From ultrasoft pseudopotentials to the projector augmented-wave method, *Physical review b* **59**, 1758 (1999).
- [116] G. Kang, Y. Kang, and S. Han, Influence of wave-function updates in g w calculations on titanates, *Physical Review B* **91**, 155141 (2015).

- [117] H. J. Monkhorst and J. D. Pack, Special points for brillouin-zone integrations, *Physical review B* **13**, 5188 (1976).
- [118] J. K. Burdett, T. Hughbanks, G. J. Miller, J. W. Richardson Jr, and J. V. Smith, Structural-electronic relationships in inorganic solids: powder neutron diffraction studies of the rutile and anatase polymorphs of titanium dioxide at 15 and 295 k, *Journal of the American Chemical Society* **109**, 3639 (1987).
- [119] K. K. Rao, S. N. Naidu, and L. Iyengar, Thermal expansion of rutile and anatase, *Journal of the American Ceramic Society* **53**, 124 (1970).
- [120] C. Howard, T. Sabine, and F. Dickson, Structural and thermal parameters for rutile and anatase, *Acta Crystallographica Section B: Structural Science* **47**, 462 (1991).
- [121] J. Heyd and G. E. Scuseria, Efficient hybrid density functional calculations in solids: Assessment of the heyd-scuseria-ernzerhof screened coulomb hybrid functional, *The Journal of chemical physics* **121**, 1187 (2004).
- [122] J. Heyd, G. E. Scuseria, and M. Ernzerhof, Hybrid functionals based on a screened coulomb potential, *The Journal of Chemical Physics* **118**, 8207 (2003).
- [123] J. Paier, M. Marsman, K. Hummer, G. Kresse, I. C. Gerber, and J. G. Ángyán, Screened hybrid density functionals applied to solids, *The Journal of chemical physics* **124**, 154709 (2006).
- [124] J. Heyd, J. E. Peralta, G. E. Scuseria, and R. L. Martin, Energy band gaps and lattice parameters evaluated with the heyd-scuseria-ernzerhof screened hybrid functional, *The Journal of chemical physics* **123**, 174101 (2005).
- [125] E. N. Brothers, A. F. Izmaylov, J. O. Normand, V. Barone, and G. E. Scuseria, Accurate solid-state band gaps via screened hybrid electronic structure calculations (2008).
- [126] M. Ernzerhof and G. E. Scuseria, Assessment of the perdew–burke–ernzerhof exchange–correlation functional, *The Journal of chemical physics* **110**, 5029 (1999).
- [127] V. Barone, O. Hod, J. E. Peralta, and G. E. Scuseria, Accurate prediction of the electronic properties of low-dimensional graphene derivatives using a screened hybrid density functional, *Accounts of chemical research* **44**, 269 (2011).
- [128] B. G. Janesko, T. M. Henderson, and G. E. Scuseria, Screened hybrid density

- functionals for solid-state chemistry and physics, *Physical Chemistry Chemical Physics* **11**, 443 (2009).
- [129] J. E. Moussa, P. A. Schultz, and J. R. Chelikowsky, Analysis of the heyd-scuseria-ernzerhof density functional parameter space, *The Journal of chemical physics* **136**, 204117 (2012).
- [130] M. Harb, P. Sautet, and P. Raybaud, Origin of the enhanced visible-light absorption in n-doped bulk anatase tio<sub>2</sub> from first-principles calculations, *The Journal of Physical Chemistry C* **115**, 19394 (2011).
- [131] A. J. Garza and G. E. Scuseria, Predicting band gaps with hybrid density functionals, *The journal of physical chemistry letters* **7**, 4165 (2016).
- [132] J. He and C. Franchini, Assessing the performance of self-consistent hybrid functional for band gap calculation in oxide semiconductors, *Journal of Physics: Condensed Matter* **29**, 454004 (2017).
- [133] M. Marsman, K. Hummer, G. Kresse, I. Gerber, and J. Ángyán, Erratum:“screened hybrid density functionals applied to solids”[*j. chem. phys.* 124, 154709 (2006)], *J. Chem. Phys* **125**, 249901 (2006).
- [134] T. M. Henderson, A. F. Izmaylov, G. E. Scuseria, and A. Savin, The importance of middle-range hartree-fock-type exchange for hybrid density functionals (2007).
- [135] T. M. Henderson, A. F. Izmaylov, G. E. Scuseria, and A. Savin, Assessment of a middle-range hybrid functional, *Journal of chemical theory and computation* **4**, 1254 (2008).
- [136] J. Muscat, A. Wander, and N. Harrison, On the prediction of band gaps from hybrid functional theory, *Chemical Physics Letters* **342**, 397 (2001).
- [137] T. Bredow and A. R. Gerson, Effect of exchange and correlation on bulk properties of mgo, nio, and coo, *Physical Review B* **61**, 5194 (2000).
- [138] M. Gerosa, C. Bottani, C. Di Valentin, G. Onida, and G. Pacchioni, Accuracy of dielectric-dependent hybrid functionals in the prediction of optoelectronic properties of metal oxide semiconductors: a comprehensive comparison with many-body gw and experiments, *Journal of Physics: Condensed Matter* **30**, 044003 (2017).
- [139] J. H. Skone, M. Govoni, and G. Galli, Self-consistent hybrid functional for condensed systems, *Physical Review B* **89**, 195112 (2014).

- [140] A. D. Becke, A new mixing of hartree–fock and local density-functional theories, *The Journal of chemical physics* **98**, 1372 (1993).
- [141] J. P. Perdew, M. Ernzerhof, and K. Burke, Rationale for mixing exact exchange with density functional approximations, *The Journal of chemical physics* **105**, 9982 (1996).
- [142] K. C. Ko, O. Lamiel-García, J. Y. Lee, and F. Illas, Performance of a modified hybrid functional in the simultaneous description of stoichiometric and reduced tio 2 polymorphs, *Physical Chemistry Chemical Physics* **18**, 12357 (2016).
- [143] Y.-f. Zhang, W. Lin, Y. Li, K.-n. Ding, and J.-q. Li, A theoretical study on the electronic structures of tio2: Effect of hartree-fock exchange, *The Journal of Physical Chemistry B* **109**, 19270 (2005).
- [144] T. Sander, E. Maggio, and G. Kresse, Beyond the tamm-dancoff approximation for extended systems using exact diagonalization, *Physical Review B* **92**, 045209 (2015).
- [145] X. Leng, F. Jin, M. Wei, and Y. Ma, Gw method and bethe–salpeter equation for calculating electronic excitations, *Wiley Interdisciplinary Reviews: Computational Molecular Science* **6**, 532 (2016).
- [146] S. Dancoff, Non-adiabatic meson theory of nuclear forces, *Physical Review* **78**, 382 (1950).
- [147] I. Tamm, Relativistic interaction of elementary particles, in *Selected Papers* (Springer, 1991) pp. 157–174.
- [148] M. Shishkin, M. Marsman, and G. Kresse, Accurate quasiparticle spectra from self-consistent gw calculations with vertex corrections, *Physical review letters* **99**, 246403 (2007).
- [149] X. Wang, W. Meng, and Y. Yan, Electronic band structures and excitonic properties of delafossites: A gw-bse study, *Journal of Applied Physics* **122**, 085104 (2017).
- [150] M. Bokdam, T. Sander, A. Stroppa, S. Picozzi, D. Sarma, C. Franchini, and G. Kresse, Role of polar phonons in the photo excited state of metal halide perovskites, *Scientific reports* **6**, 1 (2016).
- [151] V. Çelik and E. Mete, Range-separated hybrid exchange-correlation functional analyses of anatase tio 2 doped with w, n, s, w/n, or w/s, *Physical Review B* **86**,

- 205112 (2012).
- [152] F. Viñes, O. Lamiel-García, K. Chul Ko, J. Yong Lee, and F. Illas, Systematic study of the effect of hse functional internal parameters on the electronic structure and band gap of a representative set of metal oxides, *Journal of computational chemistry* **38**, 781 (2017).
- [153] See supplemental material at (), comparing the dispersion of conduction and valence bands near the respective band edges under GGA and HSE06(20) functional description.
- [154] S.-D. Mo and W. Ching, Electronic and optical properties of three phases of titanium dioxide: Rutile, anatase, and brookite, *Physical Review B* **51**, 13023 (1995).
- [155] A. Boonchun, P. Reunchan, and N. Umezawa, Energetics of native defects in anatase tio 2: a hybrid density functional study, *Physical Chemistry Chemical Physics* **18**, 30040 (2016).
- [156] P. Deak, B. Aradi, and T. Frauenheim, Quantitative theory of the oxygen vacancy and carrier self-trapping in bulk tio 2, *Physical Review B* **86**, 195206 (2012).
- [157] M. Dou and C. Persson, Comparative study of rutile and anatase sno2 and tio2: Band-edge structures, dielectric functions, and polaron effects, *Journal of Applied Physics* **113**, 083703 (2013).
- [158] P. Deak, B. Aradi, and T. Frauenheim, Polaronic effects in tio 2 calculated by the hse06 hybrid functional: Dopant passivation by carrier self-trapping, *Physical Review B* **83**, 155207 (2011).
- [159] M. Arroyo-de Dompablo, A. Morales-Garcia, and M. Taravillo, Dft+ u calculations of crystal lattice, electronic structure, and phase stability under pressure of tio2 polymorphs, *The Journal of chemical physics* **135**, 054503 (2011).
- [160] P. Borlido, T. Aull, A. W. Huran, F. Tran, M. A. Marques, and S. Botti, Large-scale benchmark of exchange–correlation functionals for the determination of electronic band gaps of solids, *Journal of chemical theory and computation* **15**, 5069 (2019).
- [161] A. Janotti, J. Varley, P. Rinke, N. Umezawa, G. Kresse, and C. G. Van de Walle, Hybrid functional studies of the oxygen vacancy in tio 2, *Physical Review B* **81**, 085212 (2010).
- [162] H. Lawler, J. Rehr, F. Vila, S. D. Dalosto, E. L. Shirley, and Z. H. Levine, Optical to

- uv spectra and birefringence of  $\text{SiO}_2$  and  $\text{TiO}_2$ : first-principles calculations with excitonic effects, *Physical Review B* **78**, 205108 (2008).
- [163] R. Asahi, Y. Taga, W. Mannstadt, and A. J. Freeman, Electronic and optical properties of anatase  $\text{TiO}_2$ , *Physical Review B* **61**, 7459 (2000).
- [164] G. Lucovsky, Electronic structure, amorphous morphology and thermal stability of transition metal oxide and chalcogenide alloys, *Journal of Optoelectronics and Advanced Materials* **3**, 155 (2001).
- [165] See supplemental material at (), for density of states showing the joint contribution of Ti-3d and O-2p states near the band edges.
- [166] D. W. Fischer, X-ray band spectra and molecular-orbital structure of rutile  $\text{TiO}_2$ , *Physical Review B* **5**, 4219 (1972).
- [167] H. Modrow, S. Bucher, J. Rehr, and A. Ankudinov, Calculation and interpretation of k-shell x-ray absorption near-edge structure of transition metal oxides, *Physical Review B* **67**, 035123 (2003).
- [168] W. Tang, E. Sanville, and G. Henkelman, A grid-based bader analysis algorithm without lattice bias, *Journal of Physics: Condensed Matter* **21**, 084204 (2009).
- [169] F. Karlicky and M. Otyepka, Band gaps and optical spectra from single- and double-layer fluorographene to graphite fluoride: many-body effects and excitonic states, *Annalen der Physik* **526**, 408 (2014).
- [170] D. Y. Qiu, H. Felipe, and S. G. Louie, Optical spectrum of  $\text{MoS}_2$ : many-body effects and diversity of exciton states, *Physical review letters* **111**, 216805 (2013).
- [171] B.-C. Shih, Y. Xue, P. Zhang, M. L. Cohen, and S. G. Louie, Quasiparticle band gap of  $\text{ZnO}$ : High accuracy from the conventional  $G_0W_0$  approach, *Physical review letters* **105**, 146401 (2010).
- [172] A. Thatribud, Electronic and optical properties of  $\text{TiO}_2$  by first-principle calculation (dft-gw and bse), *Materials Research Express* **6**, 095021 (2019).
- [173] C. E. Patrick and F. Giustino, Gw quasiparticle bandgaps of anatase  $\text{TiO}_2$  starting from dft+u, *Journal of Physics: Condensed Matter* **24**, 202201 (2012).
- [174] G. Giorgi, M. Palummo, L. Chiodo, and K. Yamashita, Excitons at the (001) surface of anatase: Spatial behavior and optical signatures, *Physical Review B* **84**, 073404 (2011).

- [175] See supplemental material at (), showing the convergence behaviour of optical transition energies and exciton binding energies with respect to number of occupied and virtual orbitals used in the BSE calculation.
- [176] M. Kolos and F. Karlický, Accurate many-body calculation of electronic and optical band gap of bulk hexagonal boron nitride, *Physical Chemistry Chemical Physics* **21**, 3999 (2019).
- [177] S. S. Ataei, M. R. Mohammadzadeh, and N. Seriani, Excitonic effects in the optical properties of hydrogenated anatase  $\text{TiO}_2$ , *Physical Review B* **95**, 155205 (2017).
- [178] R. Laskowski, N. E. Christensen, P. Blaha, and B. Palanivel, Strong excitonic effects in  $\text{CuAlO}_2$  delafossite transparent conductive oxides, *Physical Review B* **79**, 165209 (2009).
- [179] H. Chen, J. A. Dawson, and N. Umezawa, Anisotropic nature of anatase  $\text{TiO}_2$  and its intrinsic (001) surface electronic states, *Physical Review Applied* **4**, 014007 (2015).
- [180] See supplemental material at (), for the fatband representation of excitonic states in  $E \perp c$  direction for HSE06( $\alpha = 0.20, 0.25, 0.30$ ).
- [181] See supplemental material at (), which compares dielectric functions calculated using BSE with HSE06(20) and PBE functional starting points.
- [182] See supplemental material at (), which shows the Brillouin zone relevant for first optical peak predicted by PBE and HSE06( $\alpha$ ) starting points are indeed identical.
- [183] See supplemental material at (), for the dielectric function obtained by using PBE functional as the starting point for BSE calculation. The binding energy of excitons obtained for first peak at 3.745 eV in this case is  $93 \pm 10$  meV.
- [184] M. Gallart, T. Cottineau, B. Hönerlage, V. Keller, N. Keller, and P. Gilliot, Temperature dependent photoluminescence of anatase and rutile  $\text{TiO}_2$  single crystals: Polaron and self-trapped exciton formation, *Journal of Applied Physics* **124**, 133104 (2018).
- [185] J. Pascual, J. Camassel, and H. Mathieu, Fine structure in the intrinsic absorption edge of  $\text{TiO}_2$ , *Physical Review B* **18**, 5606 (1978).
- [186] R. Gonzalez, R. Zallen, and H. Berger, Infrared reflectivity and lattice fundamentals in anatase  $\text{TiO}_2$ , *Physical Review B* **55**, 7014 (1997).
- [187] Y.-N. Wu, J. K. Wuenschell, R. Fryer, W. A. Saidi, P. Ohodnicki, B. Chorpening, and

- Y. Duan, Theoretical and experimental study of temperature effect on electronic and optical properties of  $\text{TiO}_2$ : comparing rutile and anatase, *Journal of Physics: Condensed Matter* **32**, 405705 (2020).
- [188] H. Tang, F. Levy, H. Berger, and P. Schmid, Urbach tail of anatase  $\text{TiO}_2$ , *Physical Review B* **52**, 7771 (1995).
- [189] N. Hosaka, T. Sekiya, M. Fujisawa, C. Satoko, and S. Kurita, Uv reflection spectra of anatase  $\text{TiO}_2$ , *Journal of electron spectroscopy and related phenomena* **78**, 75 (1996).
- [190] N. Hosaka, T. Sekiya, and S. Kurita, Excitonic state in anatase  $\text{TiO}_2$  single crystal, *Journal of luminescence* **72**, 874 (1997).
- [191] Z. Wang, U. Helmersson, and P.-O. Kall, Optical properties of anatase  $\text{TiO}_2$  thin films prepared by aqueous sol-gel process at low temperature, *Thin Solid Films* **405**, 50 (2002).
- [192] H. Tang, H. Berger, P. Schmid, F. Levy, and G. Burri, Photoluminescence in  $\text{TiO}_2$  anatase single crystals, *Solid State Communications* **87**, 847 (1993).
- [193] C. Persson and A. Ferreira da Silva, Strong polaronic effects on rutile  $\text{TiO}_2$  electronic band edges, *Applied Physics Letters* **86**, 231912 (2005).
- [194] B. J. Morgan and G. W. Watson, Polaronic trapping of electrons and holes by native defects in anatase  $\text{TiO}_2$ , *Physical Review B* **80**, 233102 (2009).
- [195] N. A. Deskins and M. Dupuis, Electron transport via polaron hopping in bulk  $\text{TiO}_2$ : A density functional theory characterization, *Physical Review B* **75**, 195212 (2007).
- [196] M. Watanabe and T. Hayashi, Time-resolved study of self-trapped exciton luminescence in anatase  $\text{TiO}_2$  under two-photon excitation, *Journal of luminescence* **112**, 88 (2005).
- [197] B. Liu, L. Wen, and X. Zhao, The photoluminescence spectroscopic study of anatase  $\text{TiO}_2$  prepared by magnetron sputtering, *Materials Chemistry and Physics* **106**, 350 (2007).
- [198] D. O. Scanlon, C. W. Dunnill, J. Buckeridge, S. A. Shevlin, A. J. Logsdail, S. M. Woodley, C. R. A. Catlow, M. J. Powell, R. G. Palgrave, I. P. Parkin, *et al.*, Band alignment of rutile and anatase  $\text{TiO}_2$ , *Nature materials* **12**, 798 (2013).



- [199] Y. Wei, M. V. Tokina, A. V. Benderskii, Z. Zhou, R. Long, and O. V. Prezhdo, Quantum dynamics origin of high photocatalytic activity of mixed-phase anatase/rutile  $\text{TiO}_2$ , *The Journal of Chemical Physics* **153**, 044706 (2020).
- [200] H. G. Yang, C. H. Sun, S. Z. Qiao, J. Zou, G. Liu, S. C. Smith, H. M. Cheng, and G. Q. Lu, Anatase  $\text{TiO}_2$  single crystals with a large percentage of reactive facets, *Nature* **453**, 638 (2008).
- [201] Y. Hu, Y. Ren, G. Tang, C. Wang, M. Tang, B. Yue, and H. He, Synthesis of  $\text{Cs}_2\text{HfO}_4/\text{TiO}_2$  nanocomposites with dominant  $\text{TiO}_2$  (001) facets and related photocatalytic properties, *Chinese Journal of Chemistry* **32**, 1151 (2014).
- [202] A. Vittadini, A. Selloni, F. Rotzinger, and M. Gratzel, Structure and energetics of water adsorbed at  $\text{TiO}_2$  anatase (101) and (001) surfaces, *Physical Review Letters* **81**, 2954 (1998).
- [203] J. Pan, G. Liu, G. Q. Lu, and H.-M. Cheng, On the true photoreactivity order of (001), (010), and (101) facets of anatase  $\text{TiO}_2$  crystals, *Angewandte Chemie International Edition* **50**, 2133 (2011).
- [204] A. Selloni, Anatase shows its reactive side, *Nature Materials* **7**, 613 (2008).
- [205] X.-Q. Gong and A. Selloni, Reactivity of anatase  $\text{TiO}_2$  nanoparticles: the role of the minority (001) surface, *The Journal of Physical Chemistry B* **109**, 19560 (2005).
- [206] E. Baldini, T. Palmieri, A. Dominguez, P. Ruello, A. Rubio, and M. Chergui, Phonon-driven selective modulation of exciton oscillator strengths in anatase  $\text{TiO}_2$  nanoparticles, *Nano letters* **18**, 5007 (2018).
- [207] E. Baldini, A. Dominguez, T. Palmieri, O. Cannelli, A. Rubio, P. Ruello, and M. Chergui, Exciton control in a room temperature bulk semiconductor with coherent strain pulses, *Science advances* **5**, eaax2937 (2019).

## SUPPLEMENTAL MATERIAL

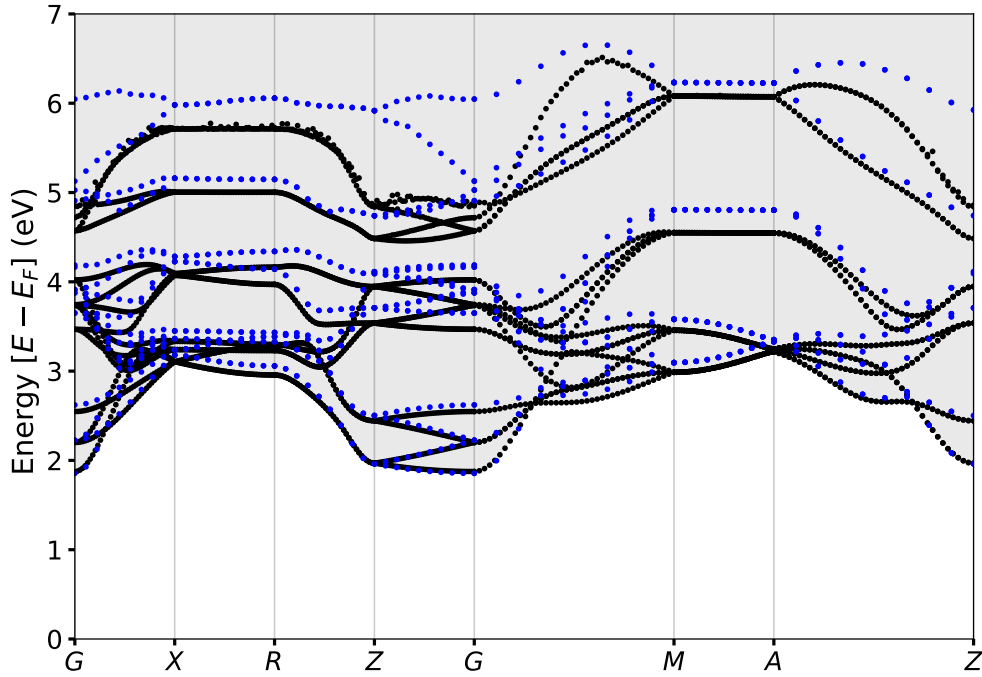


FIG. 8. Comparison of conduction band structure under PBE and modified HSE06(20) description. The black and blue dots represents the conduction band energies when PBE and HSE06(20) functionals, respectively, are used. The bands are superposed for comparing dispersion by shifting the HSE06(20) conduction bands uniformly downward so as to match its edge with the PBE conduction edge. Valance band has similar dispersion in both PBE and HSE06(20) description for the exchange correlation, hence not shown here. The general trend we observe is that the dispersion of bands in PBE and HSE06(20) cases agrees with each other in energy ranges very close to the band edges. The agreement worsens further away from the edge.

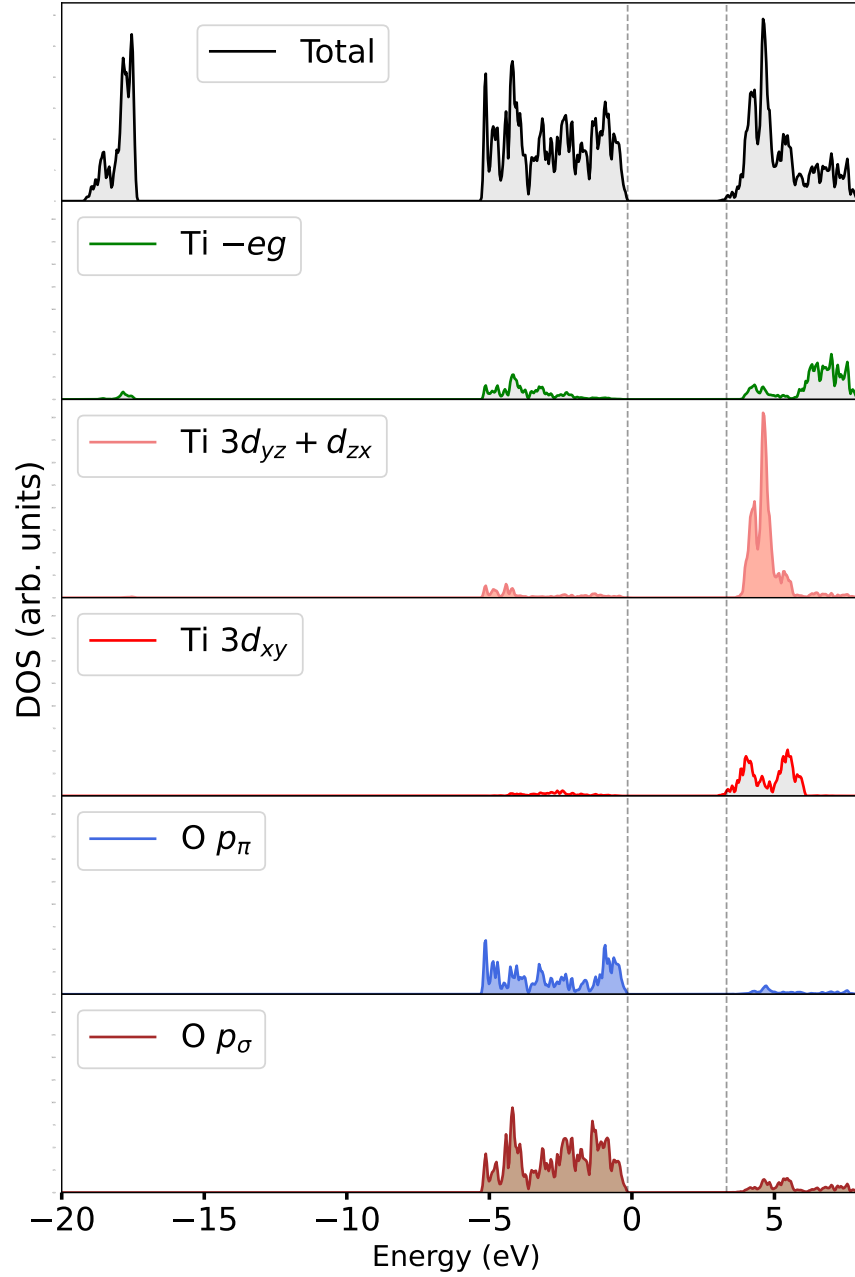


FIG. 9. Total and projected density of states of the anatase TiO<sub>2</sub> structure calculated within the HSE06(20) set up. The Fermi energy is taken as the zero of energy in the bandstructure. The vertical dashed lines on the left and right indicate the valence band maximum and conduction band minimum, respectively. The DOS is decomposed into Ti-*e<sub>g</sub>*, Ti-*t<sub>2g</sub>*(*d<sub>yz</sub>*, *d<sub>zx</sub>* and *d<sub>xy</sub>*), O-*p<sub>σ</sub>* in the Ti<sub>3</sub>-O cluster plane and O-*p<sub>π</sub>* out of the Ti<sub>3</sub>-O cluster plane components.

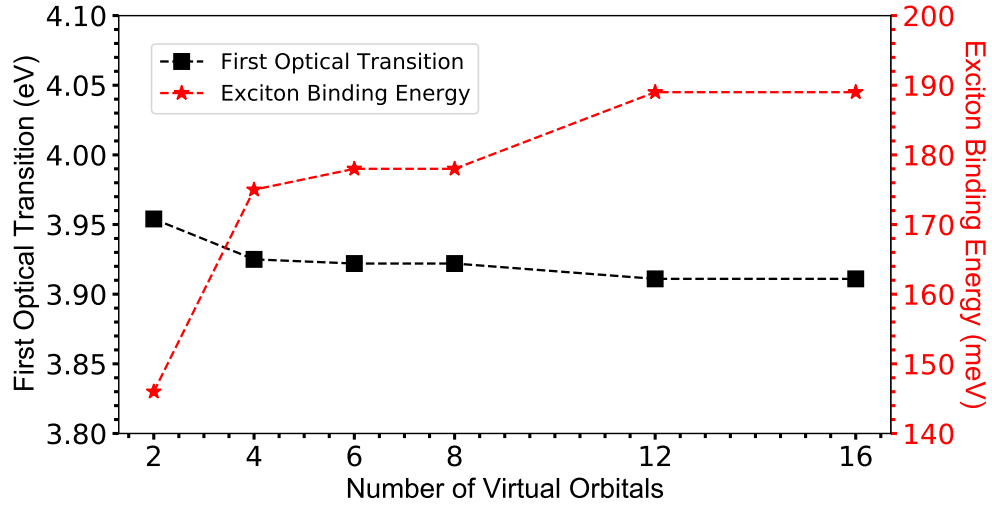


FIG. 10. Convergence behaviour of first excitonic transition and exciton binding energy with respect to number of virtual orbitals used in the BSE

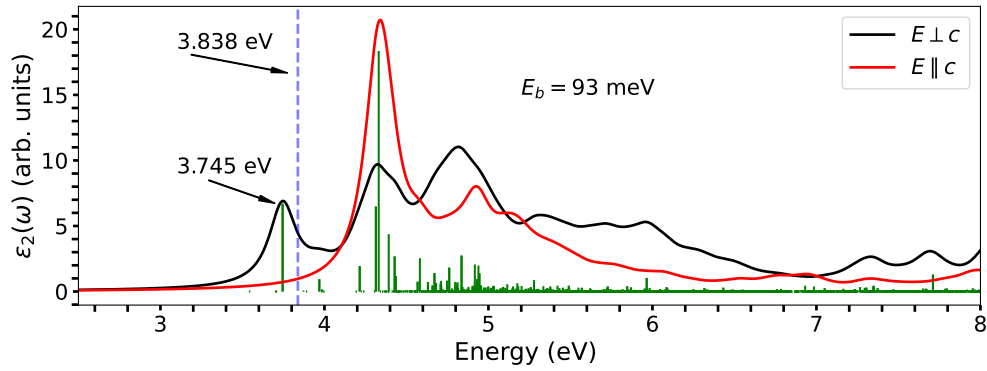


FIG. 11. Dielectric function obtained from BSE with PBE starting wavefunction

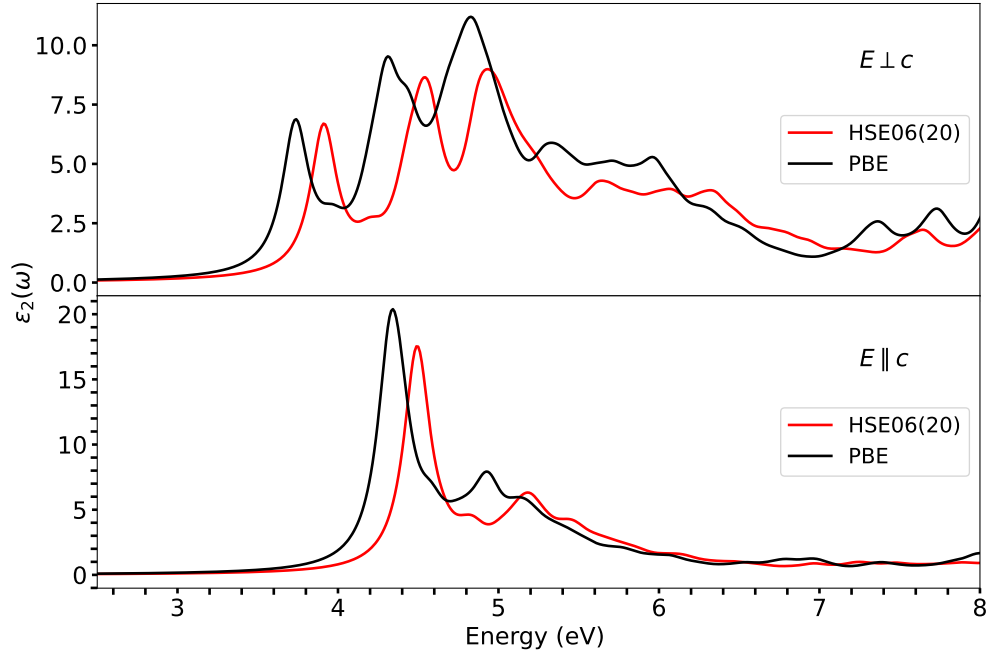


FIG. 12. Comparison of dielectric function obtained from BSE with PBE and HSE06(20) starting wavefunction

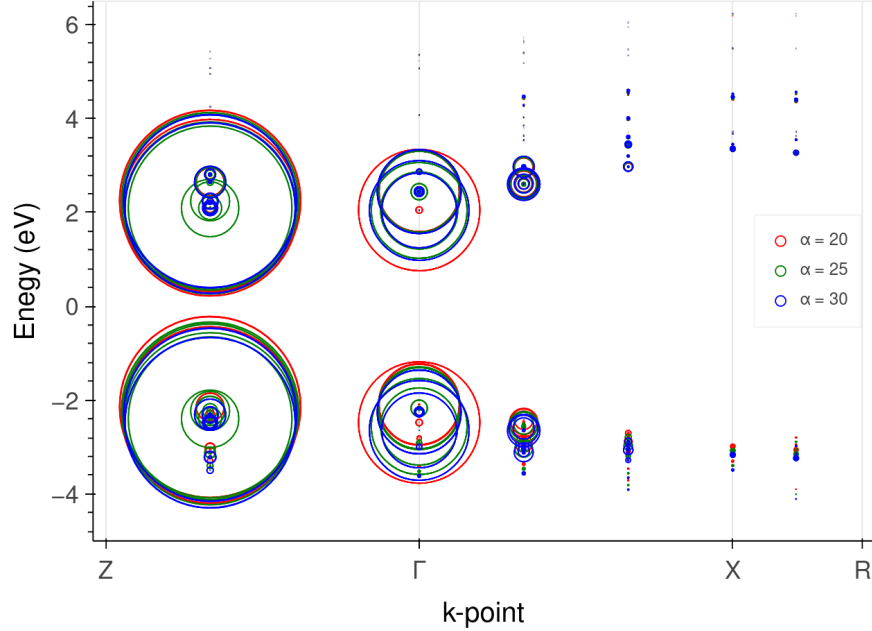


FIG. 13. Fatband representation showing region of Brillouin zone that are important for first optical peak in anatase TiO<sub>2</sub> shown for HSE06( $\alpha = 20, 25, 30\%$ ). Irrespective of the value of  $\alpha$ , the region of Brillouin zone at which transitions occur and exciton coupling coefficient are similar(except for small change in the energies of individual excitons).

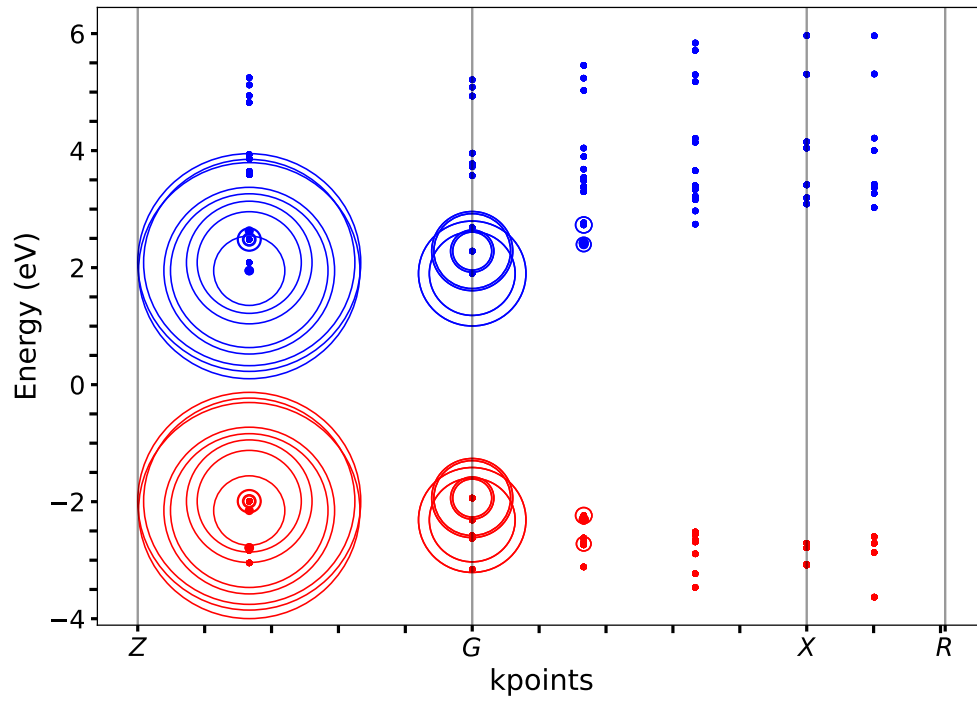


FIG. 14. Projection of excitonic amplitudes on the quasiparticle bandstructure near the band edges obtained for PBE starting wavefunction.